

## VARIATIONAL DISCRETIZATION FOR ROTATING STRATIFIED FLUIDS

MATHIEU DESBRUN

Applied Geometry Lab, Computing + Mathematical Sciences, Caltech  
1200 E. California Blvd, Pasadena, CA 91125, USA

EVAN S. GAWLIK

Computational and Mathematical Engineering, Stanford University  
450 Serra Mall, Stanford, CA 94305-2004, USA

FRANÇOIS GAY-BALMAZ

CNRS/LMD, École Normale Supérieure, Paris, France  
24, Rue Lhomond, 75005 Paris

VLADIMIR ZEITLIN

LMD, École Normale Supérieure, UPMC, Paris, France  
24, Rue Lhomond, 75005 Paris

(Communicated by the associate editor name)

**ABSTRACT.** In this paper we develop and test a structure-preserving discretization scheme for rotating and/or stratified fluid dynamics. The numerical scheme is based on a finite dimensional approximation of the group of volume preserving diffeomorphisms recently proposed in [25, 9] and is derived via a discrete version of the Euler-Poincaré variational formulation of rotating stratified fluids. The resulting variational integrator allows for a discrete version of Kelvin circulation theorem, is applicable to irregular meshes and, being symplectic, exhibits excellent long term energy behavior. We then report a series of preliminary tests for rotating stratified flows in configurations that are symmetric with respect to translation along one of the spatial directions. In the benchmark processes of hydrostatic and/or geostrophic adjustments, these tests show that the slow and fast component of the flow are correctly reproduced. The harder test of inertial instability is in full agreement with the common knowledge of the process of development and saturation of this instability, while preserving energy nearly perfectly and respecting conservation laws.

**1. Introduction.** Numerical simulations of rotating stratified flows are of obvious importance in modeling atmospheric and oceanic dynamics at different spatial and temporal scales, and are being massively and routinely performed. In spite of constant progress in numerical schemes which are successfully used for this purpose,

---

2010 *Mathematics Subject Classification.* Primary: 37M15, 37N10; Secondary: 65P10, 37K65.

*Key words and phrases.* Rotating stratified fluids, geometric discretization, Euler-Poincaré formulation, structure-preserving schemes, hydrostatic and geostrophic adjustments.

This research was partially supported by a “Projet Incitatif de Recherche” contract from the Ecole Normale Supérieure de Paris, by the Swiss NSF grant 200020-137704, by the U.S. NSF grant CCF-1011944, and by the U.S. Department of Energy grant DE-FG02-97ER25308.

the respect of the intrinsic structure of the equations of fluid motion is rarely discussed or addressed while developing and/or implementing new codes. Yet, in the limit of infinite Reynolds (or Péclet) number, which is relevant for e.g. large-scale atmospheric or oceanic flows [26], the equations of motion of the stratified rotating fluid possess a specific geometric structure [28]—as do the related Euler equations [2, 3]. Physically, this structure manifests itself in specific Lagrangian conservation laws, the most celebrated being the conservation of potential vorticity which alone allows one to understand many processes taking place in the atmosphere, the ocean, or in laboratory experiments (e.g. [16]). We remind the reader that potential vorticity, whose Lagrangian conservation follows from Ertel’s theorem, is a quantity constructed by projecting the absolute (i.e. relative plus planetary, which is due to rotation) vorticity onto the density gradient and dividing the result by the total density. Conservation of potential vorticity follows from Kelvin’s circulation theorem [10]. The existence of a variational (Hamilton’s) principle allows one to interpret this circulation theorem in terms of the general Noether theorem, linking conservation laws to symmetries. Conservation of potential vorticity, thus, is related to the symmetry with respect to Lagrangian particle relabeling [28]. One should recall that so-called balanced models in geophysical fluid dynamics, like the famous quasigeostrophic model [26] (which are extensively used to understand large-scale atmospheric and ocean dynamics as well as in climate modeling [23]) are an expression of potential vorticity conservation in a certain range of scales. They too possess a (reduced) variational principle [14]. On the other hand, the (non-canonical) Hamiltonian structure of the fluid dynamics equations suggests the use of so-called symplectic integrators [11] allowing for very accurate long-term conservation of energy.

The question of relevance of the accurate representation of the conservation laws in a numerical scheme, which should eventually simulate a forced-dissipative real world, is often debated—but has never been systematically investigated. Some studies comparing simulation with structure-preserving and standard schemes do show differences [19], [1]. We believe that capturing conservation laws is in fact numerically crucial, especially in the context of large-scale atmosphere and ocean dynamics at extremely high Reynolds numbers, as well as for long-time climatic simulations.

In this paper, we develop and test a structure-preserving space-time discretization scheme for rotating and/or stratified fluid dynamics. In order to achieve this goal, we use a recently developed structure-preserving discretization for the incompressible Euler equations and its extension to incompressible fluids with advected quantities [25, 9], together with the geometric interpretation of the dynamics of ideal rotating and/or stratified fluids via Euler-Poincaré variational principles [13]. We will limit ourselves in this paper to models that are symmetric with respect to translations along one of the spatial directions configurations (so-called 2.5 dimensional systems).

The paper is organized as follows. In Section 2, we recall the theory of continuous and discrete Euler-Poincaré formulations, the construction of the discrete diffeomorphism group, and the derivation of the associated structure-preserving discretization of Euler equations. In Section 3 we derive a structure-preserving discretization for two-dimensional non-rotating stratified fluids. We then give a geometric Euler-Poincaré formulation of rotating non-stratified (Section 4), and rotating stratified (Section 5) fluids in the 2.5 dimensional situation and use this formulation to derive

a structure-preserving discretization. We finally present tests of our new numerical schemes in Section 6.

**2. Continuous and discrete Euler-Poincaré equations.** Our approach is based on a few essential ingredients. First, we leverage the geometric interpretation (and its underlying variational principle) of the flow of an ideal incompressible fluid as a geodesic on the group of volume-preserving diffeomorphisms of the domain of the flow [2]. This key geometric picture is known to extend to the case where additional fields are advected by the flow [13], yet interact with it through body forces. Second, we rely on *symplectic integrators* [11], obtained via extremization of variational principles [22], to numerically ensure good energy behavior as well as exact conservation laws due to Noether's theorem. Finally, we adopt the construction of a consistent spatial discretization of the group of volume preserving diffeomorphism recently proposed in [25], as well as its further developments for incompressible continuum theories [9].

In this section we first recall the formal theory of Euler-Poincaré reduction with advected quantities and the associated circulation theorem, both at the continuous and discrete level. We then review the construction of the discrete volume preserving diffeomorphism group together with the resulting variational integrator for the Euler equations of an ideal fluid.

**2.1. Euler-Poincaré theory with advection.** From the work of Arnold (see, e.g., [2]), it is well known that the flow of the Euler equations of an ideal fluid of constant density describes a geodesic on the group of volume preserving diffeomorphisms of the domain of the fluid, relative to a right invariant  $L^2$  Riemannian metric. More precisely, let us denote by  $M \subset \mathbb{R}^n$  the domain of the fluid (supposed to be compact and with smooth boundary) and denote by  $\text{Diff}_{vol}(M)$  the group of all volume preserving diffeomorphisms  $M$ . The motion of an incompressible fluid is completely characterized by a curve  $\varphi_t \in \text{Diff}_{vol}(M)$ : a particle located at a point  $X$  at time  $t = 0$  travels to  $x = \varphi_t(X)$  at time  $t$ . The equations of motion can naturally be derived from Hamilton's variational principle

$$\delta \int_0^T L(\varphi, \dot{\varphi}) dt = 0, \quad \text{where} \quad L(\varphi, \dot{\varphi}) = \frac{1}{2} \int_M |\dot{\varphi}|^2 dV.$$

As this Lagrangian is invariant under particle relabeling, that is, the action of  $\text{Diff}_{vol}(M)$  on itself by composition on the right, the variational principle can be rewritten in terms of the Eulerian velocity  $\mathbf{u}(x, t)$  verifying  $\dot{\varphi}(X) = \mathbf{u}(\varphi_t(X), t)$ , i.e.  $\mathbf{u} = \dot{\varphi} \circ \varphi^{-1}$ . One then obtains the following constrained variational principle

$$\delta \int_0^T \ell(\mathbf{u}) dt = 0, \quad \text{where} \quad \ell(\mathbf{u}) = \frac{1}{2} \int_M |\mathbf{u}|^2 dV,$$

subject to constrained variations  $\delta \mathbf{u} = \dot{\mathbf{v}} - [\mathbf{v}, \mathbf{u}]$ , where  $\mathbf{v}$  is an arbitrary divergence free vector field and  $[\cdot, \cdot]$  is the vector field commutator.

In order to implement the variational integrator based on the discretization of the diffeomorphism group, it will be crucial to understand the relation between the Lagrangian and the Eulerian variational principle from a more abstract point of view. This is done by using the theory of Euler-Poincaré reduction, see [21], valid for any  $G$ -invariant Lagrangian system on a Lie group  $G$ . Taking  $G = \text{Diff}_{vol}(M)$  recovers Arnold's formulation of ideal fluids, and explains the associated variational principle.

In the context of geophysical fluid dynamics, there is a new element related to the density or (potential) temperature fluctuations interacting with velocity field. In what follows we will use the Boussinesq approximation where these fluctuations are advected by the flow. Yet, they are coupled to the velocity field through gravity. The abstract formalism allowing for such a more general situation has been described in [13] and will be of crucial use to derive a variational integrator, as has been done in [9]. The Euler-Poincaré theory with advected quantities is briefly reviewed below.

2.1.1. *Continuous theory.* Let  $G$  be a Lie group acting on the right on a vector space  $V$ . We will denote by

$$(g, v) \in G \times V \mapsto vg \in V \quad \text{and} \quad (g, a) \in G \times V^* \mapsto ag \in V^*,$$

the action of  $G$  on  $V$  and its dual  $V^*$ . The associated infinitesimal actions of the Lie algebra  $\mathfrak{g}$  of  $G$  are defined by

$$v\xi := \left. \frac{d}{dt} \right|_{t=0} v \exp(t\xi) \quad \text{and} \quad a\xi := \left. \frac{d}{dt} \right|_{t=0} a \exp(t\xi)$$

for  $\xi \in \mathfrak{g}$ ,  $v \in V$ ,  $a \in V^*$ , and where  $\exp : \mathfrak{g} \rightarrow G$  denotes the exponential map of the Lie group  $G$ .

In application to incompressible fluids in a domain  $M$ , the group  $G$  is the group  $\text{Diff}_{vol}(M)$  of all volume preserving diffeomorphisms of  $M$  and the space  $V$  is such that its dual space contains the variables advected by the flow such as buoyancy, entropy, or magnetic field, on which the diffeomorphism group acts by pullback. The Lie algebra  $\mathfrak{g}$  of  $\text{Diff}_{vol}(M)$  is the space  $\mathfrak{X}_{div}(M)$  of divergence-free vector fields on  $M$ , and its dual may be identified with  $\Omega^1(M)/d\Omega^0(M)$ , the space of one-forms on  $M$  modulo full differentials.

We now recall from [13] the Euler-Poincaré reduction process with advected quantities. Note that in this paper, we will apply this formalism to fluids both at the continuous and the discrete level, that is, when the group  $G$  is the infinite dimensional group of volume preserving diffeomorphisms or the finite dimensional group of discrete volume preserving diffeomorphisms. It is therefore crucial to formulate this reduction process in the abstract setting, that is, for an arbitrary Lie group  $G$ . Moreover, this formalism allows us to describe an abstract Kelvin circulation theorem that can be applied both at the continuous and discrete levels.

**Theorem 2.1.** *Assume that the function  $L : TG \times V^* \rightarrow \mathbb{R}$  is right  $G$ -invariant, so that upon fixing  $a_0 \in V^*$ , the Lagrangian  $L_{a_0} : TG \rightarrow \mathbb{R}$  defined by  $L_{a_0}(v_g) := L(v_g, a_0)$  is right  $G_{a_0}$ -invariant, where  $G_{a_0}$  denotes the isotropy subgroup of  $a_0$ . Define  $\ell : \mathfrak{g} \times V^* \rightarrow \mathbb{R}$  by*

$$\ell(v_g g^{-1}, a_0 g^{-1}) = L(v_g, a_0).$$

*Given a curve  $g(t)$  in  $G$ , define  $\xi(t) := \dot{g}(t)g(t)^{-1} \in \mathfrak{g}$  and  $a(t) = a_0 g(t)^{-1} \in V^*$ . Then the following are equivalent:*

- i. *With  $a_0$  held fixed, Hamilton's variational principle*

$$\delta \int_0^T L_{a_0}(g(t), \dot{g}(t)) dt = 0,$$

*holds, for variations  $\delta g(t)$  of  $g(t)$  vanishing at the endpoints.*

- ii.  *$g(t)$  satisfies the Euler-Lagrange equations for  $L_{a_0}$  on  $G$ .*

iii. *The constrained variational principle*

$$\delta \int_0^T \ell(\xi(t), a(t)) dt = 0,$$

holds on  $\mathfrak{g} \times V^*$ , upon using variations of the form

$$\delta \xi = \frac{\partial \eta}{\partial t} - [\xi, \eta], \quad \delta a = -a\eta,$$

where  $\eta(t) \in \mathfrak{g}$  vanishes at the endpoints.

iv. *The following Euler-Poincaré equations hold on  $\mathfrak{g} \times V^*$ :*

$$\frac{\partial}{\partial t} \frac{\delta \ell}{\delta \xi} = -\text{ad}_\xi^* \frac{\delta \ell}{\delta \xi} + \frac{\delta \ell}{\delta a} \diamond a, \quad (1)$$

where  $\diamond : V^* \times V \rightarrow \mathfrak{g}^*$  is the bilinear operator defined by

$$\langle v \diamond a, \xi \rangle = -\langle a\xi, v \rangle, \quad \text{for all } v \in V, a \in V^*, \text{ and } \xi \in \mathfrak{g}.$$

2.1.2. *The Kelvin-Noether theorem.* The Kelvin-Noether theorem is a version of Noether's theorem that holds for solutions of the Euler-Poincaré equations. In particular, a direct application of this theorem to the Euler equations gives rise to Kelvin's circulation theorem. We provide here the abstract formulation of the Kelvin-Noether theorem, following [13]. Let  $G$  be a Lie group which acts from the left on a manifold  $\mathcal{C}$  and suppose that  $\mathcal{K} : \mathcal{C} \times V^* \rightarrow \mathfrak{g}^{**}$  is an equivariant map, that is

$$\langle \mathcal{K}(g^{-1}c, ag), \text{Ad}_g^* \mu \rangle = \langle \mathcal{K}(c, a), \mu \rangle, \quad \text{for all } g \in G, c \in \mathcal{C}, a \in V^*, \text{ and } \mu \in \mathfrak{g}^*.$$

Let  $g(t)$ ,  $\xi(t)$ ,  $a(t)$  be solutions of the Euler-Poincaré equation (1) with an initial advected parameter  $a_0$ ; further define  $c(t) := g(t)c_0$  and

$$I(t) := \left\langle \mathcal{K}(c(t), a(t)), \frac{\delta \ell}{\delta \xi}(t) \right\rangle. \quad (2)$$

Then we have the conservation law

$$\frac{d}{dt} I(t) = \left\langle \mathcal{K}(c(t), a(t)), \frac{\delta \ell}{\delta a} \diamond a(t) \right\rangle. \quad (3)$$

In the case of the incompressible Euler equations, the Lie group is  $G = \text{Diff}_{\text{vol}}(M)$  and there is no advected quantity  $a$ . The manifold  $\mathcal{C}$  is the space of loops in the domain  $M$  and the function  $\mathcal{K} : \mathcal{C} \rightarrow \mathfrak{X}_{\text{div}}(M)^{**}$  is

$$\langle \mathcal{K}(\gamma), \alpha \rangle = \int_\gamma \alpha, \quad (4)$$

where  $\alpha$  is a one-form in  $\Omega^1(M)/d\Omega^0(M)$ . So in this case the double dual  $\mathfrak{X}_{\text{div}}(M)^{**}$  is identified with the space of closed loops in  $M$ . With these choices (3) recovers the usual circulation theorem

$$\frac{d}{dt} \int_{\gamma_t} \mathbf{u} \cdot d\mathbf{x} = 0,$$

where  $\gamma_t$  is a loop advected by the flow.

2.1.3. *Temporal discretization of Euler-Poincaré equations and symplecticity.* We now describe, following [9], a variational integrator for the Euler-Poincaré equations (1). It is adapted from [7] to the case with advected quantities.

Consider a sequence of points  $g_0, g_1, \dots, g_K \in G$  and  $\xi_0, \xi_1, \dots, \xi_{K-1} \in \mathfrak{g}$  forming the discretization of the curves  $g(t) \in G$  and  $\xi(t) \in \mathfrak{g}$ , and fix a time step  $h$ . The relations  $\xi(t) = \dot{g}(t)g(t)^{-1}$  and  $a(t) = a_0g(t)^{-1}$  are discretized as

$$\xi_k = \tau^{-1}(g_{k+1}g_k^{-1})/h \quad \text{and} \quad a_k = a_0g_k^{-1},$$

where  $\tau : \mathfrak{g} \rightarrow G$  is a local approximant of the exponential map. Such a map  $\tau$  is called a group difference map if it is a local diffeomorphism taking a neighborhood of  $0 \in \mathfrak{g}$  to a neighborhood of  $e \in G$ , with  $\tau(0) = e$  and  $\tau(\xi)^{-1} = \tau(-\xi)$ . Given  $\xi \in \mathfrak{g}$ , we denote by  $d\tau_\xi : \mathfrak{g} \rightarrow \mathfrak{g}$  the right trivialized tangent map defined as

$$d\tau_\xi(\delta) := (\mathbf{D}\tau(\xi) \cdot \delta) \tau(\xi)^{-1}, \quad \delta \in \mathfrak{g}.$$

We use  $d\tau_\xi^{-1} : \mathfrak{g} \rightarrow \mathfrak{g}$  to refer to the inverse of this map, and  $(d\tau_\xi^{-1})^* : \mathfrak{g}^* \rightarrow \mathfrak{g}^*$  for the dual map.

The discrete analogue of the action

$$s^{a_0}(g(t)) = \int_0^T \ell(\xi(t), a(t)) dt$$

is given by

$$s_d^{a_0}((g_k)_{k=0}^K) = \sum_{k=0}^{K-1} \ell(\xi_k, a_k) h,$$

and the discrete Euler-Poincaré equations are obtained by applying the following discrete variational principle

$$\delta s_d^{a_0}((g_k)_{k=0}^K) = 0, \quad (5)$$

for arbitrary variations  $\delta g_k$  of  $g_k$  such that  $\delta g_0 = \delta g_K = 0$ .

**Theorem 2.2.** *Let  $\ell : \mathfrak{g} \rightarrow \mathbb{R}$  be a Lagrangian,  $h$  a time step and  $\tau : \mathfrak{g} \rightarrow G$  a group difference map. Then the discrete variational principle (5) yields the update equations*

$$\begin{cases} (d\tau_{-h\xi_k}^{-1})^* \frac{\delta \ell}{\delta \xi_k} = (d\tau_{h\xi_{k-1}}^{-1})^* \frac{\delta \ell}{\delta \xi_{k-1}} + h \frac{\delta \ell}{\delta a_k} \diamond a_k \\ a_{k+1} = a_k \tau(-h\xi_k). \end{cases} \quad (6)$$

Being variational, this scheme yields a symplectic integrator, as explained in [22], [9].

2.1.4. *Discrete Kelvin-Noether theorem.* The discrete analogue of the quantity  $I(t)$  defined in (2) is given by

$$I_k := \left\langle \mathcal{K}(c_k, a_k), (d\tau_{-h\xi_k}^{-1})^* \frac{\delta \ell}{\delta \xi_k} \right\rangle$$

and the discrete Kelvin-Noether theorem reads as follows:

**Theorem 2.3.** *Suppose that the sequence  $g_k, \xi_k, a_k$  satisfies the discrete Euler-Poincaré equations (6), and define  $c_k := c_0 g_k^{-1}$ . Then the quantity  $I_k$  satisfies*

$$\frac{I_k - I_{k-1}}{h} = \left\langle \mathcal{K}(c_k, a_k), \frac{\delta \ell}{\delta a_k} \diamond a_k \right\rangle.$$

We refer to [9] for a proof and more explanations.

**2.2. Discretization of the diffeomorphism group.** In order to apply the above temporal discretization for numerical simulations of fluid flows, it is necessary to further discretize the diffeomorphism group  $\text{Diff}_{vol}(M)$  by substituting it with a finite dimensional matrix Lie group. This approach, initiated in [25], is recalled here.

Given a mesh  $\mathbb{M}$  on the fluid domain  $M$  with cells  $C_i$ ,  $i = 1, \dots, N$ , define a diagonal  $N \times N$  matrix  $\Omega$  consisting of cell volumes:  $\Omega_{ii} = \text{Vol}(C_i)$ . In [25] it is shown that an appropriate choice of a group to represent discrete volume preserving diffeomorphisms is the matrix group

$$\mathcal{D}(\mathbb{M}) = \{q \in \text{GL}(N)^+ \mid q \cdot \mathbf{1} = \mathbf{1} \quad \text{and} \quad q^T \Omega q = \Omega\}, \quad (7)$$

i.e.,  $\Omega$ -orthogonal, signed stochastic matrices. Here  $\mathbf{1}$  denotes the column  $(1, \dots, 1)^T$  so that the first condition reads  $\sum_{j=1}^N q_{ij} = 1$  for all  $i = 1, \dots, N$ .

We now explain the main idea behind this definition. Consider the linear action of  $\text{Diff}_{vol}(M)$  on the space  $\mathcal{F}(M)$  of functions on  $M$ , given by

$$f \in \mathcal{F}(M) \mapsto f \circ \varphi^{-1} \in \mathcal{F}(M), \quad \varphi \in \text{Diff}_{vol}(M). \quad (8)$$

The two key properties of this linear map are the following:

- (1) it preserves the  $L^2$  inner product of functions;
- (2) it preserves the constant functions:  $C \circ \varphi^{-1} = C$ .

In the discrete setting, a function is replaced by a vector  $F \in \mathbb{R}^N$ , whose value  $F_i$  on cell  $C_i$  is regarded as the cell average of the continuous function. Therefore, the discrete  $L^2$  inner product of two discrete functions is defined by

$$\langle F, G \rangle_0 = F^T \Omega G = \sum_{i=1}^N F_i \Omega_{ii} G_i.$$

The discrete diffeomorphism group (7) is such that its action on discrete functions, i.e. on  $\mathbb{R}^N$ , by matrix multiplication, is an approximation of the linear map (8). It is simple to verify that the conditions  $q \cdot \mathbf{1} = \mathbf{1}$  and  $q^T \Omega q = \Omega$  are the discrete analogues of the conditions (1) and (2) above.

The Lie algebra of  $\mathcal{D}(\mathbb{M})$ , denoted  $\mathfrak{d}(\mathbb{M})$ , is the space of  $\Omega$ -antisymmetric, row-null matrices:

$$\mathfrak{d}(\mathbb{M}) = \{A \in \mathfrak{gl}(N) \mid A \cdot \mathbf{1} = 0 \quad \text{and} \quad A^T \Omega + \Omega A = 0\}.$$

The matrices  $A \in \mathfrak{d}(\mathbb{M})$  are thus the discrete divergence free vector fields.

**Discrete differential forms.** As we mentioned above, a discrete function (zero-form) on the mesh is given by a vector  $F \in \mathbb{R}^N$ . We will denote by  $\Omega_d^0(\mathbb{M})$  the space of discrete functions.

A discrete 1-form on  $\mathbb{M}$  is an antisymmetric matrix  $K \in \mathfrak{so}(N)$ . The space of discrete 1-form is denoted by  $\Omega_d^1(\mathbb{M})$ . The discrete exterior derivative of a discrete function  $F$  is the discrete 1-form  $dF$  given by

$$(dF)_{ij} := F_i - F_j.$$

Similarly, discrete 2-forms in  $\Omega_d^2(\mathbb{M})$  are given by antisymmetric trilinear forms on  $\mathbb{R}^N$ . The exterior derivative of a 1-form  $K \in \Omega_d^1(\mathbb{M})$  is the discrete 2-form

$$(dK)_{ijk} := K_{ij} + K_{jk} + K_{ki}.$$

These definitions, designed to enforce Stokes' theorem at the discrete level, are common to most finite-dimensional notions of exterior calculus (see, e.g., [6, 4, 8]).

The discrete analogue of the  $L^2$  pairing

$$\langle \alpha, X \rangle = \int_M \alpha \cdot X \quad (9)$$

between 1-forms  $\alpha \in \Omega^1(M)$  and vector fields  $X \in \mathfrak{X}(M)$  is given by

$$\langle K, A \rangle = \text{Tr}(K^\top \Omega A), \quad K \in \Omega_d^1(\mathbb{M}), \quad A \in \mathfrak{d}(\mathbb{M}). \quad (10)$$

Recall that using the  $L^2$  pairing (9), the dual space  $\mathfrak{X}_{div}(M)^*$  can be identified with  $\Omega^1(M)/d\Omega^0(M)$ . Remarkably, this duality holds in the discrete setting, namely, using the discrete  $L^2$  pairing (10), we have (see Theorem 2.4 in [9])

$$\mathfrak{d}(\mathbb{M})^* \simeq \Omega_d^1(\mathbb{M})/d\Omega_d^0(\mathbb{M}).$$

**Adjoint and coadjoint actions, Lie derivatives.** Recall that the adjoint and coadjoint actions of the group  $\text{Diff}_{vol}(M)$  are given by pushforward and pullback by the diffeomorphism  $\varphi$ :

$$\text{Ad}_\varphi \mathbf{u} = \varphi_* \mathbf{u} \quad \text{Ad}_\varphi^* \alpha = \varphi^* \alpha,$$

where  $\mathbf{u} \in \mathfrak{X}_{div}(M)$  and  $\alpha \in \Omega^1(M)/d\Omega^0(M)$ . The Lie bracket  $[\mathbf{u}, \mathbf{v}]$  on the Lie algebra  $\mathfrak{X}_{div}(M)$  of  $\text{Diff}_{vol}(M)$  is minus the usual Jacobi-Lie bracket of vector fields

$$[\mathbf{u}, \mathbf{v}] = \text{ad}_\mathbf{u} \mathbf{v} = \left. \frac{d}{dt} \right|_{t=0} \text{Ad}_{\varphi_t} \mathbf{v} = \left. \frac{d}{dt} \right|_{t=0} (\varphi_t)_* \mathbf{v} = -\mathcal{L}_\mathbf{u} \mathbf{v},$$

where  $\mathcal{L}_\mathbf{u} \mathbf{v}$  is the Lie derivative of  $\mathbf{v}$  along  $\mathbf{u}$ .

In the discrete setting, that is, for the group  $\mathcal{D}(\mathbb{M})$ , we have the equivalent formulas

$$\text{Ad}_q A = q A q^{-1} \quad \text{Ad}_q^* K = q^{-1} K \Omega q \Omega^{-1}. \quad (11)$$

The discrete Lie derivatives of vector fields and 1-forms are thus

$$\mathcal{L}_A B = -[A, B] = -(AB - BA) \quad \mathcal{L}_A K = -[A, K \Omega] \Omega^{-1}. \quad (12)$$

**Discrete loops.** Recall that in the continuous case, the double dual space  $\mathfrak{X}_{div}(M)^{**}$  was identified with the closed loops in  $M$  via the pairing

$$\langle \gamma, \alpha \rangle = \oint_\gamma \alpha,$$

where  $\gamma : S^1 \rightarrow M$  is a closed loop in  $M$  and  $\alpha \in \mathfrak{X}_{div}(M)^* = \Omega^1(M)/d\Omega^0(M)$ . In the discrete case, since the space  $\mathfrak{d}(\mathbb{M})$  is finite dimensional, we can simply identify the double dual  $\mathfrak{d}(\mathbb{M})^{**}$  with itself, and consider  $\mathfrak{d}(\mathbb{M})^{**}$  as the space of discrete loops. This is consistent with Arnold's treatment of Kelvin circulation theorem, see [5], [25]. The discrete analogue of (4) is thus given by

$$\langle \mathcal{K}(\Gamma), K \rangle = \langle \Gamma, K \rangle, \quad \Gamma \in \mathfrak{d}(\mathbb{M})^{**}, \quad K \in \Omega_d^1(\mathbb{M})/d\Omega_d^0(\mathbb{M}). \quad (13)$$

**Nonholonomic constraints.** For a smooth curve  $q(t) \in \mathcal{D}(\mathbb{M})$ , the matrix  $A(t) = \dot{q}(t)q(t)^{-1}$  describes the infinitesimal exchanges of fluid particles between any pairs of cells  $C_i$  and  $C_j$ . For computational efficiency, we further assume that  $A_{ij}$  is non-zero *only* if cells  $C_i$  and  $C_j$  share a common boundary. This defines a constrained set  $\mathcal{S} \subset \mathfrak{d}(\mathbb{M})$ ,

$$\mathcal{S} = \{A \in \mathfrak{d}(\mathbb{M}) \mid A_{ij} \neq 0 \Rightarrow j \in N(i)\}, \quad (14)$$

where  $N(i)$  denotes the set of indices of adjacent cells to cell  $C_i$ . Since the Lie bracket of  $A, B \in \mathcal{S}$  is not necessarily in  $\mathcal{S}$ , this constraint is nonholonomic. This

constraint will affect the variational principle, since it imposes the use of constrained variations. The standard Euler-Poincaré variational principle

$$\delta \int_0^T \ell(A) dt = 0, \quad \text{for variations } \delta A = \partial_t B + [B, A]$$

must therefore be replaced by

$$\delta \int_0^T \ell(A) dt = 0, \quad \text{with } A \in \mathcal{S} \text{ and} \tag{15}$$

for variations  $\delta A = \partial_t B + [B, A]$ ,  $B \in \mathcal{S}$ .

As shown in [25], the relation between a discrete vector field  $A \in \mathcal{S}$  and the corresponding continuous vector field  $\mathbf{u} \in \mathfrak{X}_{div}(M)$  is

$$A_{ij} \simeq -\frac{1}{2\Omega_{ii}} \int_{D_{ij}} \mathbf{u} \cdot \mathbf{n}_{ij} dS, \tag{16}$$

where  $D_{ij}$  is the boundary common to cell  $i$  and  $j$  and  $\mathbf{n}_{ij}$  is the normal vector field on  $D_{ij}$  pointing from  $C_i$  to  $C_j$ .

**The flat map.** A major issue of the discrete approach is to find an approximation of the  $L^2$  inner product of divergence free vector fields. In view of the approach we use, it is more convenient to work on an arbitrary Riemannian manifold  $M$  with metric  $g$ . In this setting, the  $L^2$  inner product reads

$$\int_M g(\mathbf{u}, \mathbf{v}) d\mathbf{x} = \int_M \mathbf{u}^b \cdot \mathbf{v} d\mathbf{x} = \langle \mathbf{u}^b, \mathbf{v} \rangle,$$

where  $\mathbf{u}^b$  is the 1-form associated to the vector field  $\mathbf{u}$  with the Riemannian metric  $g$ . Therefore, an approximation of the  $L^2$  inner product can be found through the introduction of a discrete flat operator. If we denote by  $\mathbb{M}_\varepsilon$  a mesh with resolution  $\varepsilon$ , a discrete flat operator is defined as an operator  $\flat : \mathcal{S} \subset \mathfrak{d}(\mathbb{M}) \rightarrow \Omega_d^1(\mathbb{M})$  satisfying

$$\begin{aligned} \langle A_\varepsilon^b, B_\varepsilon \rangle &\rightarrow \langle \mathbf{u}, \mathbf{v} \rangle \\ \langle A_\varepsilon^b, [B_\varepsilon, C_\varepsilon] \rangle &\rightarrow \langle \mathbf{u}, [\mathbf{v}, \mathbf{w}] \rangle \\ \langle A^b, B \rangle &= \langle B^b, A \rangle, \end{aligned}$$

for any  $A_\varepsilon, B_\varepsilon, C_\varepsilon \in \mathcal{S}$  that respectively approximate the continuous vector fields  $\mathbf{u}, \mathbf{v}, \mathbf{w}$ , where the limit above is taken as  $\varepsilon \rightarrow 0$ .

**2.3. Review of the discrete Euler equations.** As we already recalled earlier, the Euler equations

$$\partial_t \mathbf{u} + \mathbf{u} \cdot \nabla \mathbf{u} = -\nabla p \tag{17}$$

can be obtained by Euler-Poincaré theory (Theorem 2.1) for the group  $G = \text{Diff}_{vol}(M)$  and for the Lagrangian  $\ell : \mathfrak{g} = \mathfrak{X}_{div}(M) \rightarrow \mathbb{R}$  given by

$$\ell(\mathbf{u}) = \frac{1}{2} \int_M |\mathbf{u}|^2 d\mathbf{x}.$$

In view of the discrete approach used below, it is important to consider the equations (17) as written on a general Riemannian manifold  $M$ , with Riemannian metric  $g$ . In this case,  $\nabla \mathbf{u}$  is the Levi-Civita covariant derivative of  $\mathbf{u}$  associated to the metric and  $\nabla p$  is the gradient of  $p$ , taken relative to the Riemannian metric.

Note that the Euler equations (17) can be equivalently written as

$$\partial_t \mathbf{u}^b + \mathcal{L}_{\mathbf{u}} \mathbf{u}^b = -dq, \quad (18)$$

where  $\mathbf{u}^b$  is the 1-form associated to  $\mathbf{u}$  using the Riemannian metric on  $M$ ,  $\mathcal{L}_{\mathbf{u}} \mathbf{u}^b$  is the Lie derivative of the one-form  $\mathbf{u}^b$ , and  $q = p - \frac{1}{2}|\mathbf{u}|^2$ . The equivalence of (17) and (18) follows from the identity

$$\mathcal{L}_{\mathbf{u}} \mathbf{u}^b = \mathbf{u} \cdot \nabla \mathbf{u}^b + \frac{1}{2} d|\mathbf{u}|^2.$$

**Spatial discretization.** Spatial discretization of the Euler equation is obtained by considering the discrete Lagrangian  $\ell : \mathfrak{d}(\mathbb{M}) \rightarrow \mathbb{R}$ ,

$$\ell(A) = \frac{1}{2} \langle A^b, A \rangle. \quad (19)$$

Applying the Euler-Poincaré variational principle with nonholonomic constraints (15), we get the equations

$$\left( \partial_t A^b + \mathcal{L}_A A^b + dP \right)_{ij} = 0 \quad (20)$$

for all  $i, j$ , such that  $j \in N(i)$ . More explicitly, using (12), this reads

$$\partial_t A_{ij}^b + [A^b \Omega, A]_{ij} \frac{1}{\Omega_{jj}} = -(P_i - P_j), \quad j \in N(i).$$

**Temporal discretization.** The discrete Euler-Poincaré equations (6) applied to the discrete diffeomorphism group  $\mathcal{D}(\mathbb{M})$  and the Lagrangian (19) yields the update equations

$$\left( (d\tau_{-hA_k}^{-1})^* A_k^b - (d\tau_{hA_{k-1}}^{-1})^* A_{k-1}^b + dP_k \right)_{ij} = 0, \quad (21)$$

where  $\tau$  is a group difference map. A convenient and computationally efficient choice for  $\tau$  is the Cayley transform

$$\tau : \mathfrak{d}(\mathbb{M}) \rightarrow \mathcal{D}(\mathbb{M}), \quad \tau(A) = \left( I - \frac{A}{2} \right)^{-1} \left( I + \frac{A}{2} \right) \quad (22)$$

and one verifies the formulas

$$(d\tau_A^{-1})^* K = \left( I - \frac{1}{2} \mathcal{L}_A \right) K - \frac{1}{4} AK \Omega A \Omega^{-1},$$

so that (21) reads

$$\left( \frac{A_k^b - A_{k-1}^b}{h} + \frac{\mathcal{L}_{A_k} A_k^b + \mathcal{L}_{A_{k-1}} A_{k-1}^b}{2} + \frac{h}{4} \left( A_{k-1} A_{k-1}^b \Omega A_{k-1} \Omega^{-1} - A_k A_k^b \Omega A_k \Omega^{-1} \right) + dP_k \right)_{ij} = 0.$$

As explained in [9], cubic terms (matrix products involving three elements of  $\mathfrak{d}(\mathbb{M})$ ) can be ignored in the above equations, without altering the discrete Kelvin-Noether theorem that still holds exactly. The discrete equations then reduce to

$$\left( \frac{A_k^b - A_{k-1}^b}{h} + \frac{\mathcal{L}_{A_k} A_k^b + \mathcal{L}_{A_{k-1}} A_{k-1}^b}{2} + dP_k \right)_{ij} = 0.$$

**The discrete Kelvin-Noether theorem.** We now apply Theorem 2.3 to the case of the Euler equations. Let  $\mathcal{C} = \mathfrak{d}(\mathbb{M})^{**} = \mathfrak{d}(\mathbb{M}) \ni \Gamma$  be the space of discrete loops in  $\mathbb{M}$  and let  $\mathcal{D}(\mathbb{M})$  act on  $\mathcal{C}$  by discrete pullback  $\Gamma \cdot q = q^{-1} \Gamma q$ , see (11). Recall

from (13) that the quantity  $\mathcal{K} : \mathcal{C} \rightarrow \mathfrak{g}^{**}$  is given by  $\mathcal{K}(\Gamma) = \Gamma$ . So, the discrete Kelvin-Noether Theorem 2.3 says that the quantity

$$I_k = \left\langle \Gamma_k, (d\tau_{-hA_k}^{-1})^* A_k^{\flat} \right\rangle$$

verifies

$$I_k = I_{k-1},$$

where  $\Gamma_k = \Gamma_0 \cdot q_k^{-1}$  is a discrete loop advected by the discrete fluid flow.

**The case of a 2D Cartesian grid.** We now compute (20) and (21) for a 2D Cartesian grid with uniform spacing  $\varepsilon$ . Assume that the discrete vector field  $A \in \mathcal{S}$  approximates the continuous vector field  $\mathbf{u} = (u, v)$ . If  $C_i$  and  $C_j$  are horizontally adjacent cells centered at  $(a - 1/2, b + 1/2)$  and  $(a + 1/2, b + 1/2)$ , then we have

$$A_{ij} = -\frac{1}{2\varepsilon} u^{a,b+1/2}$$

If  $C_i$  and  $C_j$  are vertically adjacent cells centered at  $(a + 1/2, b - 1/2)$  and  $(a + 1/2, b + 1/2)$ , then we have

$$A_{ij} = -\frac{1}{2\varepsilon} v^{a+1/2,b}.$$

As we have seen, the Lagrangian (19) depends on the choice of an appropriate flat operator. On the 2D Cartesian grid, the operator  $\flat : \mathcal{S} \rightarrow \mathfrak{d}(\mathbb{M})$  defined by

$$A_{ij}^{\flat} := \begin{cases} 2\varepsilon^2 A_{ij} & \text{if } j \in N(i) \\ w_{ij}\varepsilon^2 \sum_{k \in N(i) \cap N(j)} (A_{ik} + A_{kj}) & \text{if } j \in N(N(i)) \end{cases} \quad (23)$$

is a discrete flat operator, where  $w_{ij} = 1$  if cells  $C_i$  and  $C_j$  share a single vertex and  $w_{ij} = 2$  if cells  $C_i$  and  $C_j$  belong to the same row or column.

Using (23) and (12), the Lie derivative is, up to an exact discrete differential,

$$\left( \mathcal{L}_A \bar{A}^{\flat} \right)_{ij} = \frac{\varepsilon}{2} (\bar{\omega}^{a,b} v^{a,b} + \bar{\omega}^{a,b+1} v^{a,b+1}) \quad (24)$$

if  $C_i$  and  $C_j$  are horizontally adjacent, and

$$\left( \mathcal{L}_A \bar{A}^{\flat} \right)_{ij} = -\frac{\varepsilon}{2} (\bar{\omega}^{a,b} u^{a,b} + \bar{\omega}^{a+1,b} u^{a+1,b}) \quad (25)$$

if  $C_i$  and  $C_j$  are vertically adjacent. We used the notations

$$u^{a,b} := \frac{u^{a,b-1/2} + u^{a,b+1/2}}{2}, \quad v^{a,b} := \frac{v^{a-1/2,b} + v^{a+1/2,b}}{2}$$

and

$$\omega^{a,b} = \frac{u^{a,b-1/2} + v^{a+1/2,b} - u^{a,b+1/2} - v^{a-1/2,b}}{\varepsilon}.$$

The spatially discretized Euler equations (20) is thus given by

$$\begin{cases} \partial_t u^{a,b+1/2} - \frac{1}{2} (\omega^{a,b} v^{a,b} + \omega^{a,b+1} v^{a,b+1}) = -\frac{1}{\varepsilon} (P^{a+1/2,b+1/2} - P^{a-1/2,b+1/2}) \\ \partial_t v^{a+1/2,b} + \frac{1}{2} (\omega^{a,b} u^{a,b} + \omega^{a+1,b} u^{a+1,b}) = -\frac{1}{\varepsilon} (P^{a+1/2,b+1/2} - P^{a+1/2,b-1/2}) \\ u^{a+1,b+1/2} + v^{a+1/2,b+1} - u^{a,b+1/2} - v^{a+1/2,b} = 0. \end{cases}$$

The fully discrete (i.e., discrete-space and discrete-time) Euler equations are given by

$$\left\{ \begin{array}{l} \frac{u_k^{a,b+1/2} - u_{k-1}^{a,b+1/2}}{h} - \frac{1}{2} \left( \frac{\omega_k^{a,b} v_k^{a,b} + \omega_k^{a,b+1} v_k^{a,b+1} + \omega_{k-1}^{a,b} v_{k-1}^{a,b} + \omega_{k-1}^{a,b+1} v_{k-1}^{a,b+1}}{2} \right) \\ \quad = -\frac{1}{\varepsilon} \left( P_k^{a+1/2,b+1/2} - P_k^{a-1/2,b+1/2} \right) \\ \frac{v_k^{a+1/2,b} - v_{k-1}^{a+1/2,b}}{h} + \frac{1}{2} \left( \frac{\omega_k^{a,b} u_k^{a,b} + \omega_k^{a+1,b} u_k^{a+1,b} + \omega_{k-1}^{a,b} u_{k-1}^{a,b} + \omega_{k-1}^{a+1,b} u_{k-1}^{a+1,b}}{2} \right) \\ \quad = -\frac{1}{\varepsilon} \left( P_k^{a+1/2,b+1/2} - P_k^{a+1/2,b-1/2} \right) \\ u_k^{a+1,b+1/2} + v_k^{a+1/2,b+1} - u_k^{a,b+1/2} - v_k^{a+1/2,b} = 0 \end{array} \right.$$

and correspond to a Crank-Nicholson time update. As explained in [25] this spatial discretization of the Euler equations on the regular grid coincides with the Harlow-Welsh scheme [12], albeit with a different time update. Therefore, the variational scheme can be seen as an extension of this approach to arbitrary grids, offering the added bonus of proving a geometric picture. Moreover, this geometric picture helps extend this scheme to important models of incompressible fluids with advected quantities, as shown in [25] and as will be done below for stratified rotating fluids, while preserving the attractive properties of the scheme such as its symplecticity, a discrete Kelvin circulation theorem, and very accurate conservation of energy.

**3. 2D stratified flow in the Boussinesq approximation.** We now start discussing generalizations of pure Eulerian fluid dynamics by including the effects of gravity and stratification (variable density). In the presence of gravity, density variations will enter the equation (17) via the buoyancy acceleration. We remind the reader that in the Boussinesq approximation the density variations with respect to some reference density value (which will be taken to be equal to unity, as in (17)) are neglected everywhere except the buoyancy term in the momentum equations. At the same time, mass conservation equations are split into two: the incompressibility equation, and the equation of advection of density fluctuations. Below we will use the full buoyancy variable  $b = g \frac{\rho}{\rho_0}$ , where  $\rho_0$  is background density,  $g$  is the gravitational acceleration, and  $\rho$  is density. The equations for incompressible two dimensional Boussinesq flows in the vertical plane thus read

$$\left\{ \begin{array}{l} \partial_t \mathbf{u} + \mathbf{u} \cdot \nabla \mathbf{u} + b \mathbf{z} = -\nabla p \\ \partial_t b + \mathbf{u} \cdot \nabla b = 0, \quad \nabla \cdot \mathbf{u} = 0 \end{array} \right. \quad (26)$$

where  $\mathbf{u} = \mathbf{u}(x, z) = (u(x, z), w(x, z))$  is the velocity,  $b = b(x, z)$  is the buoyancy,  $p = p(x, z)$  is the pressure, and  $\mathbf{z}$  is the vertical unit vector. Note that buoyancy is a Lagrangian invariant. Potential vorticity is identically zero for such system, as vorticity is perpendicular to the  $(x, z)$ -plane.

Due to the presence of the buoyancy term in the first equation in (26), a straightforward linearization around the rest state with constant background stratification (vertical gradient of buoyancy) gives rise to the linear wave solutions—*internal gravity waves*.

**3.1. Geometric formulation.** The configuration space for the two dimensional Boussinesq flow is the group  $G = \text{Diff}_{\text{vol}}(M)$  of volume preserving diffeomorphisms

of the vertical domain  $M$  under consideration. The buoyancy  $b$  is the advected parameter on which the diffeomorphism group acts on the right by composition:

$$b \cdot \varphi := b \circ \varphi.$$

The space  $V^*$  of the general theory (Theorem 2.1) is therefore identified with the space  $\mathcal{F}(M)$  of all functions on  $M$ , and the infinitesimal action and diamond operation are thus given by

$$b \cdot \mathbf{u} = \mathbf{u} \cdot \nabla b \quad \text{and} \quad v \diamond b = b \nabla v.$$

The fluid Lagrangian  $\ell : \mathfrak{g} \times V^* \rightarrow \mathbb{R}$  is the fluid's total kinetic energy minus the potential energy:

$$\ell(\mathbf{u}, b) = \int_M \left( \frac{1}{2} |\mathbf{u}|^2 - bz \right) dx dz.$$

Using the equalities

$$\frac{\delta \ell}{\delta \mathbf{u}} = \mathbf{u}, \quad \frac{\delta \ell}{\delta b} = -z, \quad \frac{\delta \ell}{\delta b} \diamond b = -z \diamond b = -b \nabla z = -b \mathbf{z},$$

one verifies that the Euler-Poincaré equations (1) produce the system (26) (see [13]).

Kelvin's circulation theorem reads

$$\frac{d}{dt} \oint_{\gamma_t} \mathbf{u} \cdot d\mathbf{x} = - \oint_{\gamma_t} b dz.$$

It is obtained from the abstract formulation (3) by choosing for  $\mathcal{C}$  the space of loops in  $M$  and the quantity  $\mathcal{K} : \mathcal{C} \times V^* \rightarrow \mathfrak{g}^{**}$  given by

$$\langle \mathcal{K}(\gamma, b), \mathbf{v}^b \rangle := \int_{\gamma} \mathbf{v}^b.$$

Indeed, one can easily compute that

$$\left\langle \mathcal{K}(\gamma, b), \frac{\delta \ell}{\delta b} \diamond b \right\rangle = - \oint_{\gamma_t} b dz.$$

**3.2. Spatial discretization.** Consider a mesh  $\mathbb{M}$  of the fluid domain  $M$ . As for the Euler equations, the spatial discretization of the Boussinesq equation is realized by replacing  $\text{Diff}_{vol}(M)$  with the finite dimensional group  $\mathcal{D}(\mathbb{M})$ , and the representation space  $\mathcal{F}(M)$  is replaced by the space  $\mathbb{R}^N$  of discrete functions on the mesh  $\mathbb{M}$ . A discrete diffeomorphism is denoted by  $q \in G = \mathcal{D}(\mathbb{M})$  and the discrete buoyancy by  $B \in V^* = \mathbb{R}^N$ . The duality pairing between  $V$  and  $V^*$  is given by the discrete  $L^2$  pairing of functions

$$\langle F, B \rangle_0 = F^\top \Omega B = \sum_{i=1}^N F_i \Omega_{ii} B_i.$$

The action by discrete pullback is given by  $B \cdot q = q^{-1} B$ , so that the infinitesimal action of a Lie algebra element  $A \in \mathfrak{d}(\mathbb{M})$  and the diamond operation respectively read

$$B \cdot A = -AB \quad \text{and} \quad F \diamond B = -(BF^\top)^\alpha, \quad B, F \in \mathbb{R}^N,$$

where  $(M)^\alpha$  denotes the skew-symmetric part of  $M$ . The diamond operation is computed as follows:

$$\begin{aligned} \langle F \diamond B, A \rangle &= -\langle B \cdot A, F \rangle_0 = \langle AB, F \rangle_0 = (AB)^\top \Omega F = B^\top A^\top \Omega F = -F^\top \Omega AB \\ &= -\text{Tr}(BF^\top \Omega A) = -\text{Tr}\left(\left(BF^\top\right)^\alpha \Omega A\right) = -\left\langle \left(BF^\top\right)^\alpha, A \right\rangle, \end{aligned}$$

where we used the fact that  $\Omega A$  for  $A \in \mathfrak{d}(\mathbb{M})$  is an antisymmetric matrix.

The spatially discretized Boussinesq Lagrangian  $\ell : \mathfrak{g} \times V^* \rightarrow \mathbb{R}$ , reads

$$\ell(A, B) = \frac{1}{2} \langle A^b, A \rangle - \langle B, Z \rangle_0, \quad (27)$$

where the discrete function  $Z \in \mathbb{R}^N$  is the discrete analogue of the coordinate  $z$ , i.e.  $Z_i$  is the height of the circumcenter of the cell  $i$ . The spatially discretized Euler-Poincaré equations associated to  $\ell(A, B)$  read

$$\begin{cases} (\partial_t A^b + \mathcal{L}_A A^b - (BZ^\top)^a + dP)_{ij} = 0 \\ \partial_t B - AB = 0, \end{cases} \quad (28)$$

for all  $i, j$ , such that  $j \in N(i)$ .

**The case of the Cartesian grid.** In this case, we choose  $Z_{a+1/2, b+1/2} = (b + 1/2)\varepsilon$ . If cell  $i$  and  $j$  are horizontally adjacent we get

$$\begin{aligned} (BZ^\top)_{ij}^a &= \frac{1}{2} \left( B^{a-1/2, b+1/2} Z^{a+1/2, b+1/2} - Z^{a-1/2, b+1/2} B^{a+1/2, b+1/2} \right) \\ &= \frac{\varepsilon}{2} (b + 1/2) \left( B^{a-1/2, b+1/2} - B^{a+1/2, b+1/2} \right) \\ &= \frac{1}{2} (Z_i B_i - Z_j B_j) = \frac{1}{2} (Q_i - Q_j). \end{aligned}$$

If cell  $i$  and  $j$  are vertically adjacent, we have instead

$$\begin{aligned} (BZ^\top)_{ij}^a &= \frac{1}{2} \left( B^{a+1/2, b-1/2} Z^{a+1/2, b+1/2} - Z^{a+1/2, b-1/2} B^{a+1/2, b+1/2} \right) \\ &= \frac{\varepsilon}{2} \left( (b + 1/2) B^{a+1/2, b-1/2} - (b - 1/2) B^{a+1/2, b+1/2} \right) \\ &= \frac{\varepsilon}{2} \left( (b - 1/2) B^{a+1/2, b-1/2} - (b + 1/2) B^{a+1/2, b+1/2} \right. \\ &\quad \left. + B^{a+1/2, b-1/2} + B^{a+1/2, b+1/2} \right) \\ &= \frac{1}{2} (Z_i B_i - Z_j B_j) + \varepsilon B^{a+1/2, b} = \frac{1}{2} (Q_i - Q_j) + \varepsilon B^{a+1/2, b}, \end{aligned}$$

where we defined the discrete function  $Q_i := Z_i B_i$  and we used the notation  $B^{a+1/2, b} := \frac{1}{2} (B^{a+1/2, b-1/2} + B^{a+1/2, b+1/2})$ .

Using the relation

$$A_{ij} = -\frac{1}{2\varepsilon} u^{a, b+1/2} \quad \text{resp.} \quad A_{ij} = -\frac{1}{2\varepsilon} w^{a+1/2, b}$$

and the formulas (24), resp. (25), we get the spatially discretized Boussinesq equations on a Cartesian grid

$$\begin{cases} \partial_t u^{a, b+1/2} - \frac{1}{2} (\omega^{a, b} w^{a, b} + \omega^{a, b+1} w^{a, b+1}) = -\frac{1}{\varepsilon} (P^{a+1/2, b+1/2} - P^{a-1/2, b+1/2}) \\ \partial_t w^{a+1/2, b} + \frac{1}{2} (\omega^{a, b} u^{a, b} + \omega^{a+1, b} u^{a+1, b}) \\ \quad + B^{a+1/2, b} = -\frac{1}{\varepsilon} (P^{a+1/2, b+1/2} - P^{a+1/2, b-1/2}) \\ u^{a+1, b+1/2} + w^{a+1/2, b+1} - u^{a, b+1/2} - w^{a+1/2, b} = 0 \\ \partial_t B^{a+1/2, b+1/2} + \frac{1}{2\varepsilon} (u^{a+1, b+1/2} B^{a+3/2, b+1/2} - u^{a, b+1/2} B^{a-1/2, b+1/2} \\ \quad + w^{a+1/2, b+1} B^{a+1/2, b+3/2} - w^{a+1/2, b} B^{a+1/2, b-1/2}) = 0. \end{cases} \quad (29)$$

**3.3. Temporal discretization.** The discrete Euler-Poincaré equations (6) applied to the discrete diffeomorphism group  $\mathcal{D}(\mathbb{M})$  and the Lagrangian (27) yields the update equations

$$\begin{cases} \left( (d\tau_{-hA_k}^{-1})^* A_k^b - (d\tau_{hA_{k-1}}^{-1})^* A_{k-1}^b - h (B_k Z^\top)^\alpha + dP_k \right)_{ij} = 0 \\ B_{k+1} = \tau(hA_k)B_k \end{cases} \quad (30)$$

or, more explicitly,

$$\begin{cases} \left( \frac{A_k^b - A_{k-1}^b}{h} + \frac{\mathcal{L}_{A_k} A_k^b + \mathcal{L}_{A_{k-1}} A_{k-1}^b}{2} - (B_k Z^\top)^\alpha + dP_k \right)_{ij} = 0 \\ B_{k+1} = \tau(hA_k)B_k, \end{cases} \quad (31)$$

where cubic terms of elements in  $\mathfrak{d}(\mathbb{M})$  have been ignored as in the Euler equations. On the 2D Cartesian grid, the first equation reads

$$\begin{cases} \frac{u_k^{a,b+1/2} - u_{k-1}^{a,b+1/2}}{h} - \frac{1}{2} \left( \frac{\omega_k^{a,b} w_k^{a,b} + \omega_k^{a,b+1} w_k^{a,b+1} + \omega_{k-1}^{a,b} w_{k-1}^{a,b} + \omega_{k-1}^{a,b+1} w_{k-1}^{a,b+1}}{2} \right) \\ \quad = -\frac{1}{\varepsilon} \left( P_k^{a+1/2,b+1/2} - P_k^{a-1/2,b+1/2} \right) \\ \frac{w_k^{a+1/2,b} - w_{k-1}^{a+1/2,b}}{h} + \frac{1}{2} \left( \frac{\omega_k^{a,b} u_k^{a,b} + \omega_k^{a+1,b} u_k^{a+1,b} + \omega_{k-1}^{a,b} u_{k-1}^{a,b} + \omega_{k-1}^{a+1,b} u_{k-1}^{a+1,b}}{2} \right) \\ \quad + B_k^{a+1/2,b} = -\frac{1}{\varepsilon} \left( P_k^{a+1/2,b+1/2} - P_k^{a+1/2,b-1/2} \right). \end{cases} \quad (32)$$

Boundary conditions fit naturally into the geometric formulation of the above numerical scheme. Tangential boundary conditions are inherent in the nonholonomic constraints (15), since neighboring cells never share an interface lying on the domain boundary. In the case of periodic boundary conditions on a Cartesian grid, we merely identify pairs of cells on opposite boundaries as neighbors in definition (14) of the nonholonomic constraint space  $\mathcal{S}$ .

These constraints are realized in implementations of (32) on a Cartesian grid of size  $N_x \times N_z$  as follows. For free-slip boundary conditions, the first relation in (32) must hold for  $1 \leq a \leq N_x - 1$ ,  $0 \leq b \leq N_z - 1$ , and the second relation must hold for  $0 \leq a \leq N_x - 1$ ,  $1 \leq b \leq N_z - 1$ , with the understanding that

$$\begin{cases} u^{0,b+1/2} = u^{N_x,b+1/2} = u^{a,-1/2} = u^{a,N_z+1/2} = 0 \\ w^{a+1/2,0} = w^{a+1/2,N_z} = w^{-1/2,b} = w^{N_x+1/2,b} = 0. \end{cases}$$

For periodic boundary conditions, (32) must hold for  $0 \leq a \leq N_x - 1$ ,  $0 \leq b \leq N_z - 1$ , with the understanding that

$$\begin{cases} P^{-1/2,b+1/2} \equiv P^{N_x-1/2,b+1/2} \\ P^{a+1/2,-1/2} \equiv P^{a+1/2,N_z-1/2} \\ B^{-1/2,b+1/2} \equiv B^{N_x-1/2,b+1/2} \\ B^{a+1/2,-1/2} \equiv B^{a+1/2,N_z-1/2} \\ u^{N_x,b+1/2} \equiv u^{0,b+1/2} \\ u^{a,-1/2} \equiv u^{a,N_z-1/2} \\ u^{a,N_z+1/2} \equiv u^{a,1/2} \\ w^{a+1/2,N_z} \equiv w^{a+1/2,0} \\ w^{-1/2,b} \equiv w^{N_x-1/2,b} \\ w^{N_x+1/2,b} \equiv w^{1/2,b}. \end{cases}$$

Mixed boundary conditions (e.g., periodic in  $x$  and tangential along the upper and lower boundaries) can be handled similarly.

**Remarks on the implementation.** Implementing the temporal update scheme involves two stages. First, compute  $B_k = \tau(hA_{k-1})B_{k-1}$  by solving the linear system

$$\left(I - \frac{hA_{k-1}}{2}\right) B_k = \left(I + \frac{hA_{k-1}}{2}\right) B_{k-1}.$$

Next, compute  $u_k$ ,  $w_k$ , and  $P_k$  by using Newton's method to solve the system of nonlinear equations consisting of (32) and the constraint

$$u_k^{a+1,b+1/2} + w_k^{a+1/2,b+1} - u_k^{a,b+1/2} - w_k^{a+1/2,b} = 0.$$

The cost of these two stages is dominated by the second, which amounts to a nonlinear solve in approximately  $3N_x N_z$  unknowns on a grid of size  $N_x \times N_z$ . Computational cost of the nonlinear solve is often reduced if the Jacobian is approximated with its incomplete LU factorization and held fixed over several Newton iterations (or even over several time steps if the flow is stable).

**Discrete circulation theorem.** Recall from (13) that the discrete circulation is given by the quantity  $\mathcal{K} : \mathcal{C} \rightarrow \mathfrak{g}^{**}$ ,  $\mathcal{K}(\Gamma) = \Gamma$ . So, the discrete Kelvin-Noether Theorem 2.3 says that the quantity

$$I_k = \left\langle \Gamma_k, (d\tau_{-hA_k}^{-1})^* A_k^b \right\rangle$$

verifies

$$\frac{I_k - I_{k-1}}{h} = \left\langle \Gamma_k, \frac{\delta \ell}{\delta B_k} \diamond B_k \right\rangle = \left\langle \Gamma_k, (B_k Z^T)^a \right\rangle,$$

where  $\Gamma_k = \Gamma_0 \cdot q_k^{-1}$  is a discrete loop advected by the discrete fluid flow.

**3.4. Including the second component of velocity.** One can include in the 2D Boussinesq equations the second component of velocity  $v$  in the  $y$ -direction as follows

$$\begin{cases} \partial_t \mathbf{u} + \mathbf{u} \cdot \nabla \mathbf{u} + b \mathbf{z} = -\nabla p \\ \partial_t v + \mathbf{u} \cdot \nabla v = 0 \\ \partial_t b + \mathbf{u} \cdot \nabla b = 0, \end{cases} \quad (33)$$

where  $\mathbf{u} = \mathbf{u}(x, z) = (u(x, z), w(x, z))$  is the velocity in the  $x$  and  $z$  direction,  $b = b(x, z)$  is the buoyancy, and  $p = p(x, z)$  is the pressure. Note that we have now

two Lagrangian invariants:  $b$  and  $v$ , and we can construct a new one, the potential vorticity, as their Jacobian.

These equations are obtained from full 3D Boussinesq equations by supposing that the flow is symmetric with respect to translations along  $y$ ; they are thus often referred to as the 2.5D Boussinesq equations. They admit an Euler-Poincaré description, by taking the same Lagrangian as above

$$\ell(\mathbf{u}, v, b) = \int_M \left( \frac{1}{2} |\mathbf{u}|^2 - bz \right) dx dz$$

without dependence on  $v$ , but using as advected quantities the buoyancy  $b = b(x, z)$  and the  $y$ -velocity  $v = v(x, z)$ , on which the diffeomorphism group acts by composition

$$b \mapsto b \circ \varphi \quad v \mapsto v \circ \varphi.$$

The spatially discretized equations are thus obtained exactly as above. We let the discrete diffeomorphism group act on the discrete buoyancy  $B \in \mathbb{R}^N$  and the discrete  $y$ -velocity  $V \in \mathbb{R}^N$  by discrete pullback,  $B \cdot q = q^{-1}B$  and  $V \cdot q = q^{-1}V$ , resulting in the following system of equations

$$\begin{cases} \left( \partial_t A^b + \mathcal{L}_A A^b - (BZ^\top)^a + dP \right)_{ij} = 0 \\ \partial_t B - AB = 0 \\ \partial_t V - AV = 0 \end{cases} \quad (34)$$

for all  $i, j$ , such that  $j \in N(i)$ .

The temporal discretization is obtained as previously presented: one simply adds to the system (31) the discrete advection equation

$$V_{k+1} = \tau(hA_k)V_k.$$

The Kelvin-Noether theorem, as well as the update equations on the Cartesian grid, are then easily derived.

**4. 2.5D rotating Euler equations.** We now concentrate on the rotation effects, excluding stratification. We work with 2.5D rotating Euler equations which are obtained from the 3D rotating Euler equations, by supposing that the flow is symmetric in one spatial direction:  $\partial_y(-) = 0$ . As the 2.5D Boussinesq equations treated above, these equations are appropriate as a first approximation while studying jets/fronts (non-rotating in the previous case, and non-stratified in the present case; we combine both effects in the next Section), which have very different along-front and across-front scales.

The resulting system reads

$$\begin{cases} \partial_t u + uu_x + wu_z - fv = -p_x \\ \partial_t v + uv_x + wv_z + fu = 0 \\ \partial_t w + uw_x + ww_z = -p_z, \end{cases} \quad (35)$$

with  $u_x + w_z = 0$  and where  $u, v, w$  depend only on  $(x, z)$ . Here  $f$  is the Coriolis parameter, i.e. twice the angular velocity of rotation, which is supposed to be around the  $z$ -axis. In order to derive a variational integrator, we rewrite these equations in an Euler-Poincaré form. This is achieved by using the geostrophic

momentum  $m := fv + f^2x$  instead of the horizontal velocity  $v$ . In terms of  $m$ , we get the system

$$\begin{cases} \partial_t u + uu_x + wu_z - m = -q_x \\ \partial_t w + uw_x + ww_z = -q_z \\ \partial_t m + um_x + wm_z = 0, \end{cases} \quad (36)$$

(see e.g. [24]), where  $q = p + \frac{1}{2}f^2x^2$ . Note that  $m$  is a Lagrangian invariant. The  $x$ -derivative of  $m$  is also a Lagrangian invariant and represents the potential vorticity for this translationally symmetric system. The equations are now identical (upon identifying  $m$  with  $-b$ ) to the Boussinesq equations (26). The internal gravity waves of the latter become *gyroscopic* (or inertial) waves in the rotating Euler equations.

Thus, (36) can be obtained by Euler-Poincaré reduction associated to the Lagrangian

$$\ell(\mathbf{u}, m) = \int \left( \frac{1}{2} |\mathbf{u}|^2 + mx \right) dx dz,$$

where  $\mathbf{u} = (u, w)$ .

Kelvin's circulation theorem,

$$\frac{d}{dt} \oint_{\gamma_t} \mathbf{u} \cdot d\mathbf{x} = \oint_{\gamma_t} m dx,$$

is obtained from the abstract formulation (3) by choosing for  $\mathcal{C}$  the space of loops in  $M$  and the quantity  $\mathcal{K} : \mathcal{C} \times V^* \rightarrow \mathfrak{g}^{**}$  given in (4). In terms of the original variables, it reads

$$\frac{d}{dt} \oint_{\gamma_t} \mathbf{u} \cdot d\mathbf{x} = \oint_{\gamma_t} fv dx.$$

It is now possible to discretize these equations in the same way as the Boussinesq equations, by using the spatially discretized Lagrangian

$$\ell(A, M) = \frac{1}{2} \langle A^b, A \rangle + \langle M, X \rangle_0,$$

where now the discrete function  $X \in \mathbb{R}^N$  is the discrete analogue of the coordinate  $x$ . The spatially discretized Euler-Poincaré equations associated to  $\ell(A, M)$  read

$$\begin{cases} \left( \partial_t A^b + \mathcal{L}_A A^b + (MX^\top)^a + dP \right)_{ij} = 0 \\ \partial_t M - AM = 0, \end{cases} \quad (37)$$

for all  $i, j$ , such that  $j \in N(i)$ .

On a 2D Cartesian grid, we have  $X_{a+1/2, b+1/2} = (a + 1/2)\varepsilon$ . Therefore, if cell  $i$  and  $j$  are horizontally adjacent, we have

$$(MX^\top)_{ij}^a = \frac{1}{2} (Q_i - Q_j) + \varepsilon M_{a, b+1/2};$$

if cell  $i$  and  $j$  are vertically adjacent, we have instead

$$(MX^\top)_{ij}^a = \frac{1}{2} (Q_i - Q_j),$$

where  $Q_i = X_i M_i$ . Therefore, Eqs. (37) used on a regular grid read

$$\left\{ \begin{array}{l} \partial_t u^{a,b+1/2} - \frac{1}{2} (\omega^{a,b} w^{a,b} + \omega^{a,b+1} w^{a,b+1}) - M_{a,b+1/2} \\ \qquad \qquad \qquad = -\frac{1}{\varepsilon} (P^{a+1/2,b+1/2} - P^{a-1/2,b+1/2}) \\ \partial_t w^{a+1/2,b} + \frac{1}{2} (\omega^{a,b} u^{a,b} + \omega^{a+1,b} u^{a+1,b}) = -\frac{1}{\varepsilon} (P^{a+1/2,b+1/2} - P^{a+1/2,b-1/2}) \\ u^{a+1,b+1/2} + w^{a+1/2,b+1} - u^{a,b+1/2} - w^{a+1/2,b} = 0 \\ \partial_t M^{a+1/2,b+1/2} + \frac{1}{2\varepsilon} (u^{a+1,b+1/2} M^{a+3/2,b+1/2} - u^{a,b+1/2} M^{a-1/2,b+1/2} \\ \qquad \qquad \qquad + w^{a+1/2,b+1} M^{a+1/2,b+3/2} - w^{a+1/2,b} M^{a+1/2,b-1/2}) = 0. \end{array} \right. \quad (38)$$

The temporal discretization can be carried out as previously for the Boussinesq equations.

To recover the discrete evolution of the original variable  $v$ , we use a discrete version of the geostrophic momentum  $m = fv + f^2x$ , namely  $M = fV + f^2X$ , to obtain the evolution of the discrete velocity  $V$  from the evolution of  $M$ .

**5. 2.5D rotating Boussinesq equations.** We now combine the effects of stratification and rotation. Again, we apply the Boussinesq approximation and assume a configuration rotating with the angular velocity  $f/2$  around the  $z$ -axis and invariant with respect to translations in  $y$ -direction. We thus get:

$$\left\{ \begin{array}{l} \partial_t u + uu_x + wu_z - fv = -p_x \\ \partial_t v + uv_x + wv_z + fu = 0 \\ \partial_t w + uw_x + ww_z + b = -p_z \\ \partial_t b + ub_x + wb_z = 0, \end{array} \right. \quad (39)$$

with  $u_x + w_z = 0$ .

The same change of variable as before,  $m = fv + f^2x$ , yields the equations

$$\left\{ \begin{array}{l} \partial_t u + uu_x + wu_z - m = -q_x \\ \partial_t w + uw_x + ww_z + b = -q_z \\ \partial_t m + um_x + wm_z = 0 \\ \partial_t b + ub_x + wb_z = 0 \end{array} \right. \quad (40)$$

with  $u_x + w_z = 0$  and where the modified pressure is  $q = p + \frac{1}{2}f^2x^2$ . Note that there are two Lagrangian invariants  $b$  and  $m$ . The third one, potential vorticity, can be constructed as the Jacobian of these two. Again, straightforward linearization reveals the presence of linear wave solutions, which are *internal inertia-gravity waves*.

The equations (40) can be obtained as Euler-Poincaré equations for the Lagrangian

$$\ell(\mathbf{u}, m, b) = \int \left( \frac{1}{2} |\mathbf{u}|^2 + mx - bz \right) dx dz,$$

where  $\mathbf{u} = (u, w)$ . In this case, there are two advected quantities,  $m$  and  $b$  on which the group  $\text{Diff}_{\text{vol}}(M)$  of volume preserving diffeomorphisms acts by composition on the right:

$$m \cdot \varphi = m \circ \varphi, \quad b \cdot \varphi = b \circ \varphi.$$

Kelvin's circulation theorem reads

$$\frac{d}{dt} \oint_{\gamma_t} \mathbf{u} \cdot d\mathbf{x} = \oint_{\gamma_t} m dx - \oint_{\gamma_t} b dz.$$

Being in an Euler-Poincaré form, the system (40) can be spatially discretized using the Lagrangian

$$\ell(A, M, B) = \frac{1}{2} \langle A^b, A \rangle + \langle M, X \rangle_0 - \langle B, Z \rangle_0,$$

where the discrete functions  $X$  and  $Z$  have the same meaning as above. The spatially discretized Euler-Poincaré equations associated to  $\ell(A, M, B)$  read

$$\begin{cases} \left( \partial_t A^b + \mathcal{L}_A A^b - (BZ^\top)^\alpha + (MX^\top)^\alpha + dP \right)_{ij} = 0 \\ \partial_t M - AM = 0 \\ \partial_t B - AB = 0 \end{cases} \quad (41)$$

for all  $i, j$ , such that  $j \in N(i)$ .

On a 2D Cartesian grid, we get

$$\begin{cases} \partial_t u^{a,b+1/2} - \frac{1}{2} (\omega^{a,b} w^{a,b} + \omega^{a,b+1} w^{a,b+1}) - M_{a,b+1/2} \\ \quad = -\frac{1}{\varepsilon} (P^{a+1/2,b+1/2} - P^{a-1/2,b+1/2}) \\ \partial_t w^{a+1/2,b} + \frac{1}{2} (\omega^{a,b} u^{a,b} + \omega^{a+1,b} u^{a+1,b}) + B_{a+1/2,b} \\ \quad = -\frac{1}{\varepsilon} (P^{a+1/2,b+1/2} - P^{a+1/2,b-1/2}) \\ u^{a+1,b+1/2} + w^{a+1/2,b+1} - u^{a,b+1/2} - w^{a+1/2,b} = 0 \\ \partial_t M^{a+1/2,b+1/2} + \frac{1}{2\varepsilon} (u^{a+1,b+1/2} M^{a+3/2,b+1/2} - u^{a,b+1/2} M^{a-1/2,b+1/2} \\ \quad + w^{a+1/2,b+1} M^{a+1/2,b+3/2} - w^{a+1/2,b} M^{a+1/2,b-1/2}) = 0 \\ \partial_t B^{a+1/2,b+1/2} + \frac{1}{2\varepsilon} (u^{a+1,b+1/2} B^{a+3/2,b+1/2} - u^{a,b+1/2} B^{a-1/2,b+1/2} \\ \quad + w^{a+1/2,b+1} B^{a+1/2,b+3/2} - w^{a+1/2,b} B^{a+1/2,b-1/2}) = 0, \end{cases} \quad (42)$$

where

$$M^{a,b+1/2} = \frac{M^{a-1/2,b+1/2} + M^{a+1/2,b+1/2}}{2},$$

$$B^{a+1/2,b} = \frac{B^{a+1/2,b-1/2} + B^{a+1/2,b+1/2}}{2}.$$

The discrete Kelvin's (circulation) Theorem 2.3 implies that the quantity

$$I_k = \left\langle \Gamma_k, (d\tau_{-hA_k}^{-1})^* A_k^b \right\rangle$$

verifies

$$\frac{I_k - I_{k-1}}{h} = \left\langle \Gamma_k, \frac{\delta \ell}{\delta B_k} \diamond B_k + \frac{\delta \ell}{\delta M_k} \diamond M_k \right\rangle = \left\langle \Gamma_k, (B_k Z^\top)^\alpha - (M_k X^\top)^\alpha \right\rangle,$$

where  $\Gamma_k = \Gamma_0 \cdot q_k^{-1}$  is a discrete loop advected by the discrete fluid flow.

**6. Numerical tests.** We now report a series of preliminary tests of the proposed numerical scheme for the three considered configurations, namely for 2D Boussinesq equations and 2.5D rotating Euler equations (to test separately and respectively how the scheme treats stratification and rotation) and finally for 2.5D rotating Boussinesq equations (where both effects are combined). It is important to bear in mind that in all three cases the system supports internal waves. These are gravity waves in pure stratified case, inertial (or gyroscopic) waves in pure rotating case, and inertia-gravity waves in the mixed case. Waves are fast motions, and it is important that the numerical scheme resolves them well. At the same time the potential-vorticity bearing motions are slow, and the separation of slow and fast motions at small Rossby numbers is one of the paradigms of geophysical fluid dynamics, e.g. [29].

**6.1. Hydrostatic adjustment in 2D Boussinesq model.** Consider the 2D Boussinesq equations (26) in the vertical plane. If the fluid is in equilibrium, the gravitational term is balanced by the pressure term and we have the *hydrostatic balance*:

$$-b = \frac{\partial p}{\partial z}.$$

If the system is out of equilibrium (due, for example, to a localized heating), it tends to a balanced state via the process of *hydrostatic adjustment* [17] by emitting internal gravity waves.

We test our numerical scheme with the hydrostatic adjustment process. Consider the hydrostatic equilibrium  $u(x, z) = w(x, z) = 0$  and  $b(x, z) = -N^2 z$ , where  $N$  is the Brunt-Väisälä frequency. The pressure is thus given by  $p(x, z) = \frac{1}{2}gN^2 z^2$ . We now consider a localized perturbation of buoyancy. More precisely, for the buoyancy we consider the initial value

$$b_0(x, z) = -N^2 z + \tilde{b}(x, z),$$

where  $\tilde{b}(x, z)$  is a positive function with compact support around a certain point  $(x_0, z_0)$  (localized perturbation). It is known that the frequency of the emitted gravity waves verifies the dispersion relation

$$\omega^2 - \frac{k_x^2 N^2}{\mathbf{k}^2} = 0, \quad (43)$$

where  $\mathbf{k} = (k_x, k_z) \in \mathbb{Z}^2$  is the wave vector. An important properties of this dispersion relation is its anisotropy, and the fact that wave frequencies are bounded from above by  $N$ .

To test our variational integrator in this situation, we consider the equations (26) in the domain  $(x, z) \in [0, 24] \times [0, 1]$  with free-slip boundary conditions along  $[0, 24] \times \{0\}$  and  $[0, 24] \times \{1\}$ , periodicity in  $x$ , and take  $N = 1$ . The Brunt-Väisälä period, i.e. the minimal period of internal gravity waves is  $2\pi$  under this scaling. For the buoyancy perturbation, we choose the initial condition

$$\tilde{b}(x, z) = \begin{cases} -z + \beta \exp\left(\frac{-r_0^2}{r_0^2 - r^2}\right) & \text{if } r < r_0 \\ -z & \text{if } r > r_0 \end{cases} \quad (44)$$

with  $r_0 = 0.2$ ,  $\beta = 0.3$ ,  $r^2 = (x-12)^2 + (z-0.5)^2$ . Our scheme (32) was implemented on a  $384 \times 16$  grid, from  $t = 0$  to  $t = 100$  with the time step  $\Delta t = 0.5$ . Long-time energy conservation is obtained as expected (Fig. 1) due to the symplecticity of our integrator.

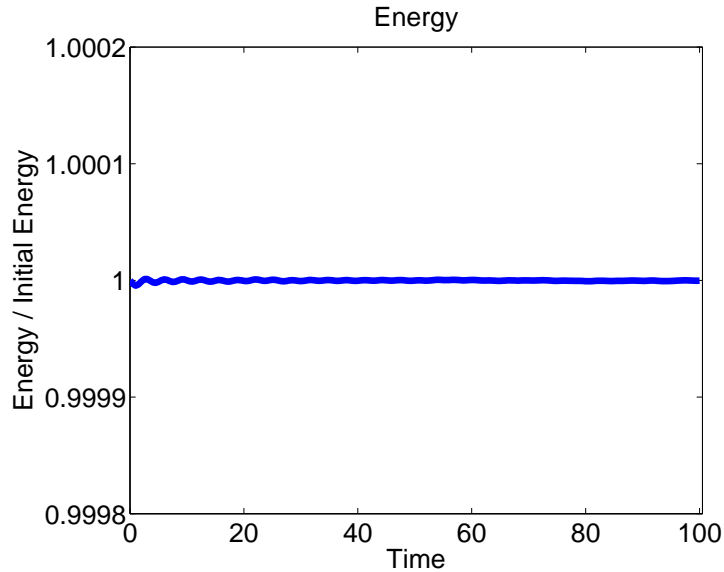


FIGURE 1. Long-time energy evolution for the hydrostatic adjustment problem in 2D Boussinesq model.

The graph Fig. 2 displays the Fourier transform of the time series of the buoyancy  $b(x, z, t)$  for  $t \in [0, 100]$  at various locations  $(x, z)$  in the domain. The integers  $i_x$  and  $i_z$  are the indices of the cell whose center is the point  $(x, z)$ , in the  $384 \times 16$  mesh of the domain  $[0, 24] \times [0, 1]$ . For instance, the cell with  $(i_x, i_z) = (192, 8)$  is near the center of the grid and its upper right corner has coordinates  $(x, z) = (12, 0.5)$ . It is clearly seen that the spectra in all locations sharply drop beyond unity, which is the non-dimensional value of  $N$ , in accordance with (43). A well pronounced maximum at unity in the middle of the domain (middle column), where the initial perturbation was located, is also consistent with (43), as the group velocity of the waves tends to zero at  $\omega \rightarrow N$  and, hence, the corresponding part of initial perturbation cannot be evacuated.

The snapshots of the evolution of the buoyancy field in the region  $[11, 13] \times [0, 1]$  which are presented in Fig. 3 confirm the wave emission from the initial perturbation. With our boundary conditions, waves are being reflected from the boundaries, but the initial stages clearly show emission from the localized source.

Finally, Fig. 4 shows the buoyancy averaged over  $0 < t < 100$ . The mean state is stably stratified and horizontally uniform as it should. We repeated the simulation with different domain geometries, all confirming the standard scenario of hydrostatic adjustment.

***Geostrophic adjustment in 2.5D rotating Euler equations.*** As mentioned in Sect. 4, 2.5D rotating Euler equations are equivalent to 2D Boussinesq equations under appropriate changes of variables, so the above-discussed simulations apply to the *geostrophic adjustment* process, i.e. adjustment of velocity and pressure to the geostrophic balance, given by the relation

$$fv = \frac{\partial p}{\partial x},$$

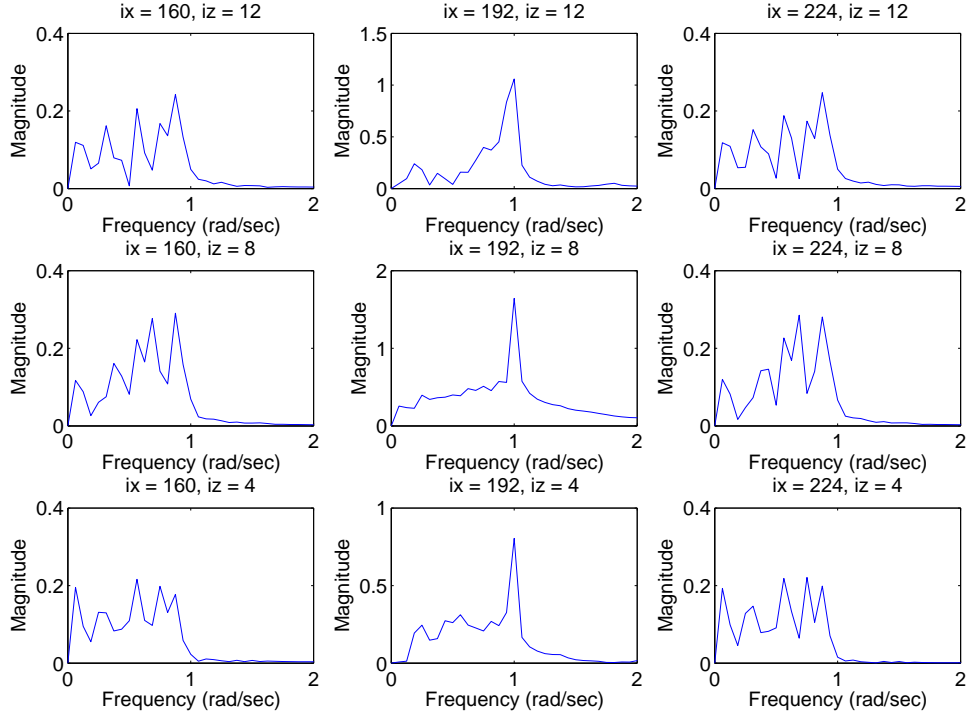


FIGURE 2. Frequency spectra of buoyancy at different locations in the flow domain for the hydrostatic adjustment problem in 2D Boussinesq model.

by emitting the gyroscopic waves with dispersion relation

$$\omega^2 = \frac{f^2 k_z^2}{|\mathbf{k}|^2}.$$

**6.2. Adjustment in the 2.5D rotating Boussinesq equations.** Consider now the equation (39). Similarly to what we have seen before, an exact solution is provided by balancing the Coriolis and gravitational terms by the pressure force (the so-called thermal wind relations):

$$fv = \frac{\partial p}{\partial x}, \quad fu = 0, \quad b = -\frac{\partial p}{\partial z}. \quad (45)$$

Such a situation is realized for example when  $u = w = 0$ ,  $v(x, z) = Kx$ ,  $b(x, z) = -N^2 z$ ,  $p = \frac{1}{2}Kx^2 + \frac{1}{2}N^2 z^2$ , with  $K$  a constant and  $N$  the Brunt-Väisälä frequency.

We consider that such equilibrium state is disturbed by a localized perturbation of the buoyancy. In this case, the frequency of the emitted wave verifies the dispersion relation

$$\omega^2 = \frac{f(K + f)k_z^2 + N^2 k_x^2}{|\mathbf{k}|^2}. \quad (46)$$

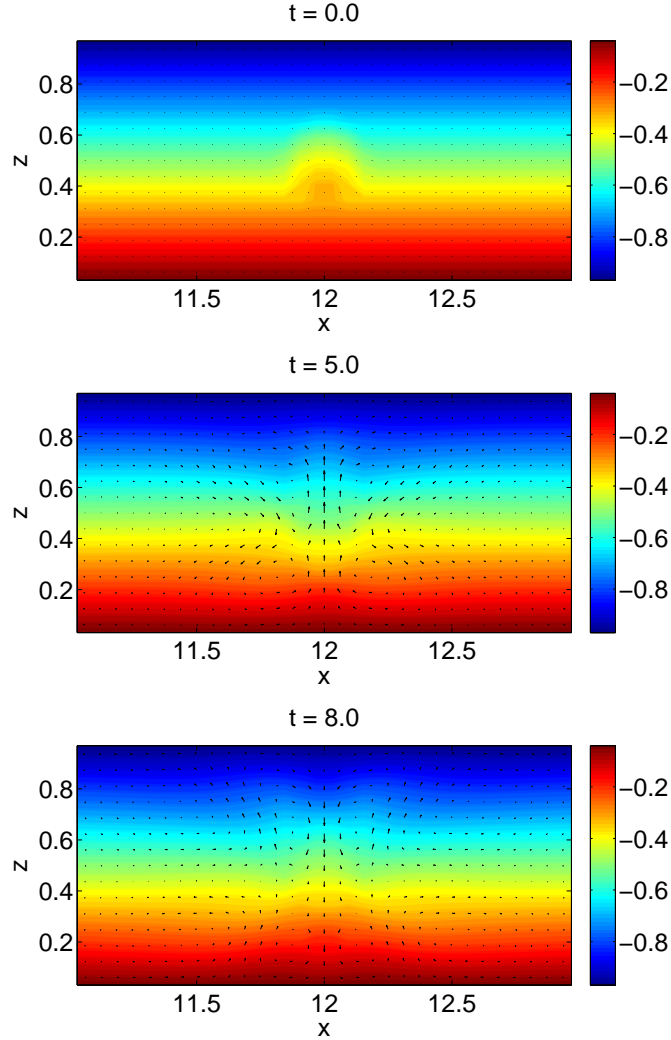


FIGURE 3. Wave emission in the buoyancy field during the hydrostatic adjustment problem in 2D Boussinesq. The corresponding animation may be viewed at <http://www.geometry.caltech.edu/Movies/BoussinesqAIMS/boussinesq4.avi>

This frequency is bounded from above and below. In the simplest case of the absence of background shear, i.e.  $K = 0$ , we have  $f < \omega < N$  (we assume  $f < N$ , which is the case of the ocean and the atmosphere).

To illustrate the behavior of our integrator in this situation, we consider the equations (39) on the domain  $(x, z) \in [-1, 2] \times [-1, 2]$ , with free-slip boundary conditions and we take  $K = 0$ ,  $f = 1$ ,  $N = 4$ . For buoyancy, we choose the same initial condition as (44), with  $r_0 = 0.2$ ,  $\beta = 0.3$ ,  $r^2 = (x - 0.5)^2 + (z - 0.5)^2$ . Our variational integrator (42) was implemented on a  $96 \times 96$  grid from  $t = 0$  to  $t = 80$  with the time step  $\Delta t = 0.2$ .

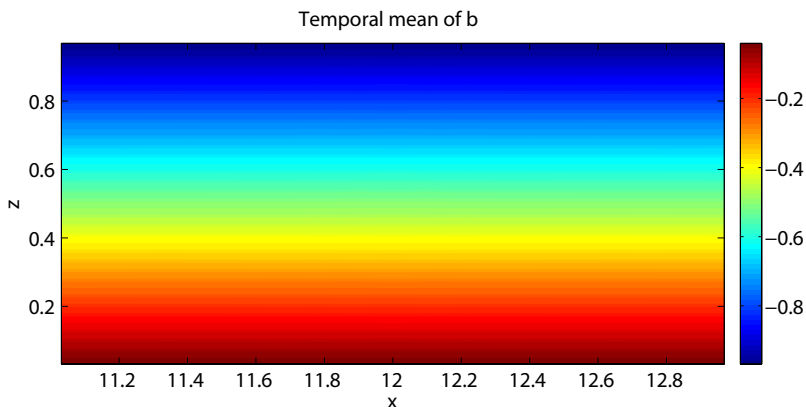


FIGURE 4. Mean of the buoyancy  $b$  during the hydrostatic adjustment process  $0 < t < 100$ .

Of course, the rigid boundaries prevent inertia-gravity waves from escaping from the domain, so the adjusted state may be expected only for time-averaged quantities, the time-averaging obviously filtering rapidly oscillating waves.

In the series of snapshots presented in Fig. 5, we display the evolution of the buoyancy perturbation  $b + N^2 z$  with superimposed velocity field  $(u, w)$  in the region  $[0, 1] \times [0, 1]$ .

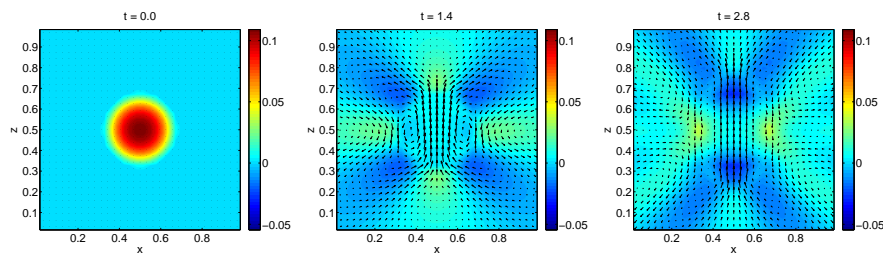


FIGURE 5. Inertia-gravity waves in the buoyancy perturbation during the geostrophic adjustment in rotating Boussinesq equations. The corresponding animation may be viewed at <http://www.geometry.caltech.edu/Movies/BoussinesqAIMS/both5b+N2z.avi>

Emission of inertia-gravity waves from the initial perturbation is clearly seen, displaying a characteristic "St. Andrew's cross" pattern [18].

The plots of Fig. 6 display the Fourier transform of the time series for the buoyancy  $b(x, z, t)$  for  $t \in [0, 80]$  at various locations  $(x, z)$  in the domain. The integers  $ix$  and  $iz$  are the indices of the cell with the center at the point  $(x, z)$ . They clearly show that the frequencies lie in the band 1, 4, i.e. between  $f$  and  $N$  in non-dimensional terms, confirming the inertia-gravity wave nature of the signal.

In the sequence of images presented in Fig. 7 the contour plots showing  $m(x, z)$  with superimposed velocity field as a function of time demonstrate the conservation of the geostrophic momentum in the scheme.

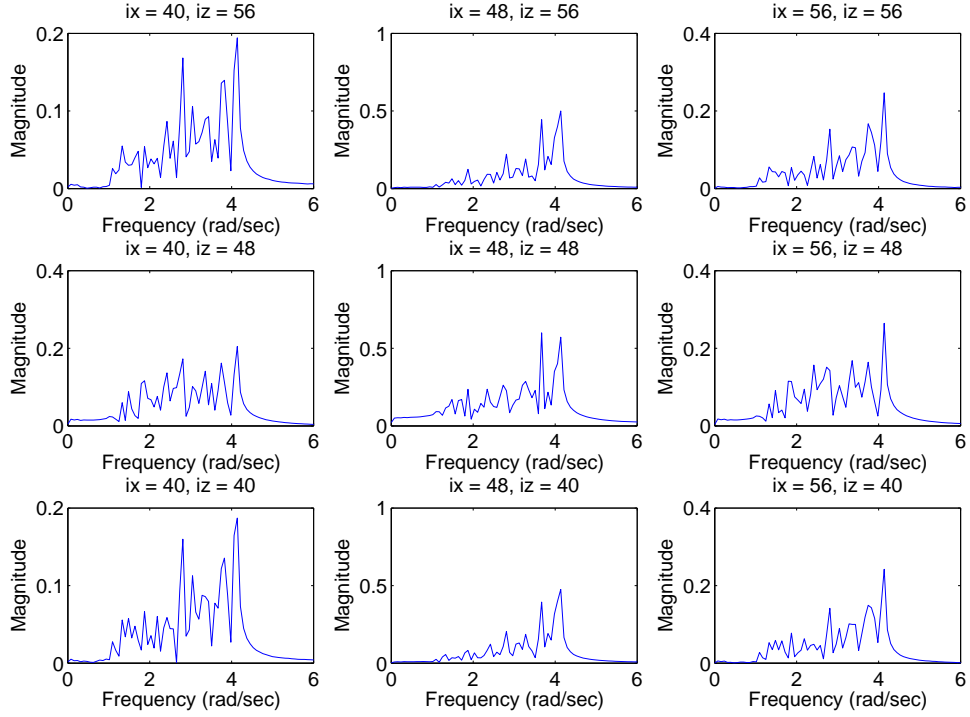


FIGURE 6. Frequency spectra of buoyancy during the geostrophic adjustment process at different locations in the domain.

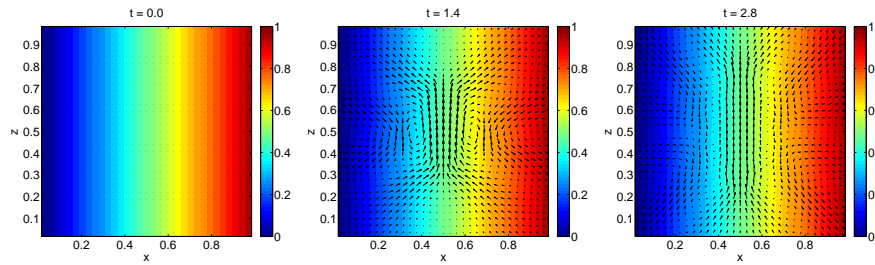


FIGURE 7. Conservation of the geostrophic momentum during the geostrophic adjustment in rotating Boussinesq equations. The corresponding animation may be viewed at <http://www.geometry.caltech.edu/Movies/BoussinesqAIMS/both5m.avi>

The graph Fig. 8 illustrates the excellent long term energy behavior, which is due to the symplecticity of our scheme.

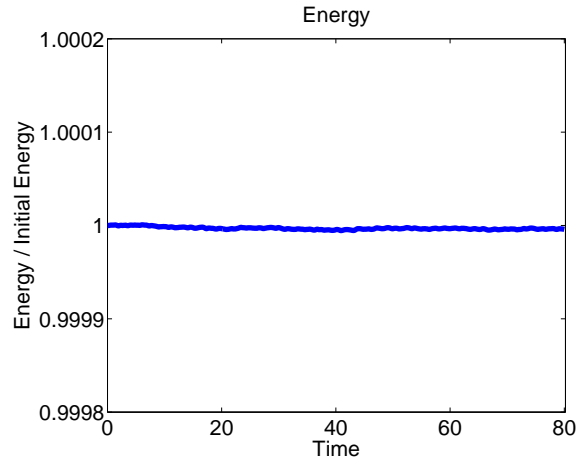


FIGURE 8. Energy conservation during the geostrophic adjustment in rotating Boussinesq equations

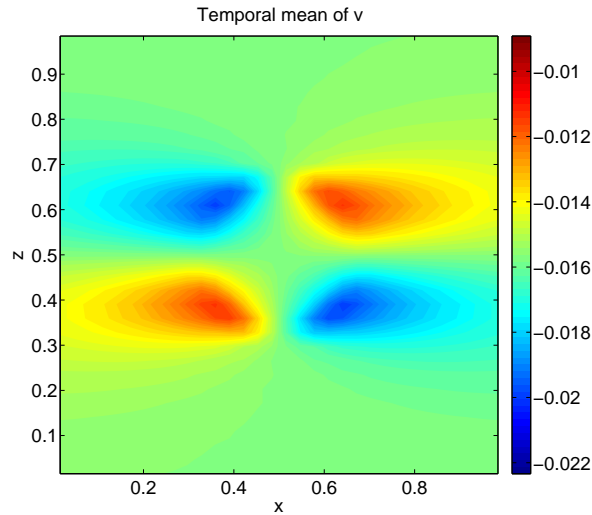


FIGURE 9. Mean  $v$  in the geostrophic adjustment process. An animation of the evolution of the velocity  $v$  during the geostrophic adjustment process may be viewed at <http://www.geometry.caltech.edu/Movies/BoussinesqAIMS/both5v.avi>

The time averages of the velocity, of the buoyancy anomaly  $b + N^2 z$  (with the background stratification removed), and the pressure anomaly  $p - \frac{1}{2} N^2 z$  (with pressure due to the basic stratification removed), over the interval  $0 < t < 80$ , are presented in Figs. 9, 10, 11. They show very good agreement with the thermal wind relation (45).

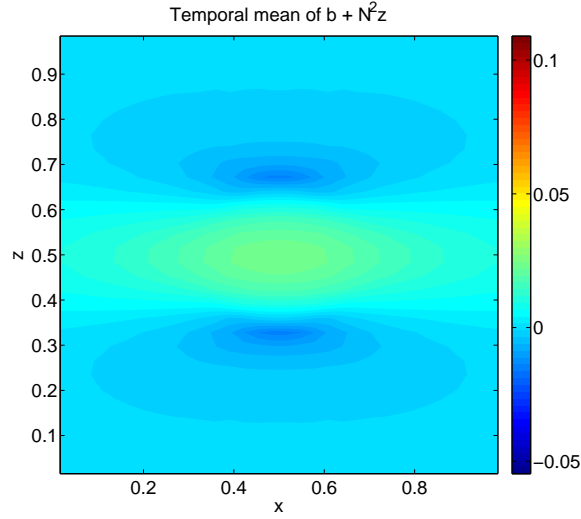


FIGURE 10. Mean buoyancy anomaly in the geostrophic adjustment process.

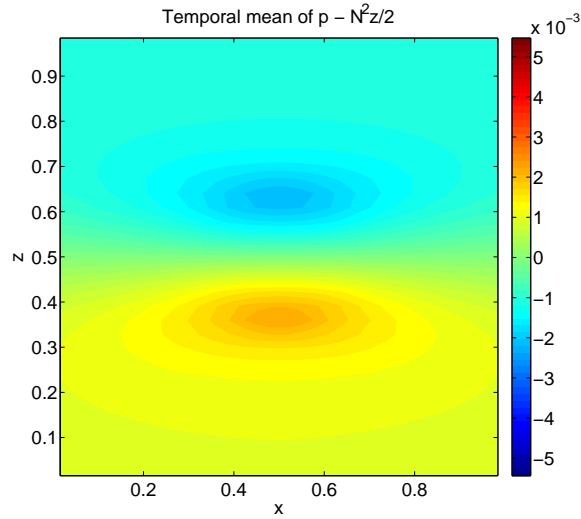


FIGURE 11. Mean pressure anomaly in the geostrophic adjustment process.

The same simulations were carried out with a localized perturbation in  $v$  instead of  $b$ , with similar results concerning long term energy behavior and the period of the emitted waves was found.

**6.3. Inertial instability in 2.5D rotating Boussinesq equations.** Having seen that the numerical scheme reproduces well the basic phenomena in the rotating 2.5 D Boussinesq equations we try in this subsection a really hard test of the inertial instability. The inertial instability is a specific instability of the rotating flows (see,

e.g., [15]) appearing in the regions where the product of planetary and potential vorticities is negative. For positive  $f$  (Northern hemisphere) we are using, this means that potential vorticity should be negative somewhere in the flow, meaning that vorticity should be sufficiently negative. Vorticity may be measured by the Rossby number of the flow. To make this parameter appear, we rewrite the 2.5D rotating Boussinesq equations (39) in a nondimensional form, that is,

$$\begin{cases} \partial_t u + \mathcal{R}(uw_x + wu_z) - v = -p_x \\ \partial_t v + \mathcal{R}(wv_x + vw_z) + u = 0 \\ \delta^2(\partial_t w + \mathcal{R}(uw_x + wv_z)) + b = -p_z \\ \partial_t b + \mathcal{R}(ub_x + wb_z) = 0, \end{cases} \quad (47)$$

with  $u_x + w_z = 0$ . Here  $\mathcal{R} = U/fL$  is the Rossby number, with  $L$  the horizontal length scale and  $U$  the horizontal velocity scale;  $\delta = H/L$  is the aspect ratio, with  $H$  the vertical length scale; and we choose  $1/f$  as the time scaling. We fix  $\delta = 1$ . In the present case, the geostrophic momentum is given by  $m(x, z) = v(x, z) + \frac{1}{\mathcal{R}}x$  and the equations may be rewritten as

$$\begin{cases} \partial_t u + \mathcal{R}(uw_x + wu_z) - m = -q_x \\ \partial_t w + \mathcal{R}(uw_x + wv_z) + b = -q_z \\ \partial_t m + \mathcal{R}(um_x + wm_z) = 0 \\ \partial_t b + \mathcal{R}(ub_x + wb_z) = 0, \end{cases} \quad (48)$$

where  $q = p + \frac{1}{2\mathcal{R}}x^2$ .

The simplest configuration where inertial instability appears is a barotropic anti-cyclonic shear with  $v(x, z) = -\tanh(x)$ . It was studied in [27], and we will consider it below.

For numerical tests, we consider the equations (48) on the domain  $(x, z) \in [-4, 4] \times [-1, 2]$ , with free-slip boundary conditions and consider the same steady solution as before:  $u(x, z) = 0$ ,  $v(x, z) = -\tanh(x)$ ,  $w(x, z) = 0$ , and  $b(x, z) = -\frac{1}{\mathcal{R}}z$ , so that  $p(x, z) = \frac{1}{2\mathcal{R}}z^2 - \ln(\cosh(x))$ . We disturb this state by a localized perturbation of  $b$  given by

$$\tilde{b}(x, z) = \begin{cases} \beta x \exp\left(\frac{-r_0^2}{r_0^2 - r^2}\right) & \text{if } r < r_0 \\ 0 & \text{if } r > r_0, \end{cases}$$

with  $r_0 = 0.2$ , and  $r^2 = x^2 + (z - 0.5)^2$ . Our variational integrator (42) was implemented on a  $32 \times 32$  grid from  $t = 0$  to  $t = 12$  with  $dt = 0.04$ . We performed simulations with the following values:  $\mathcal{R} = 1/2$ ,  $\mathcal{R} = 1$ ,  $\mathcal{R} = 2$ ,  $\mathcal{R} = 3$  and  $\beta = 0.5$ ,  $\beta = 1$ ,  $\beta = 2$ . As is easy to see the shear flow becomes inertially unstable at  $\mathcal{R} > 1$ . We give a comparison of the simulation of a stable flow with  $\mathcal{R} = 1$  and  $\beta = 1$  and unstable flow with  $\mathcal{R} = 2$  and  $\beta = 0.5$  (a lesser value of  $\beta$  is taken in this case to prevent a too rapid evolution of the instability). The snapshots of the buoyancy field  $b$  presented in Fig. 12 for the inertially stable configuration clearly illustrate how the perturbation provokes oscillations and emission of inertia-gravity waves, without reorganization of the mean flow.

The snapshots of the evolution of the buoyancy field in the simulation of the inertially unstable configuration presented in Fig. 13 clearly show the development of the instability, with a formation of ‘‘drops’’ of buoyancy anomalies with associated

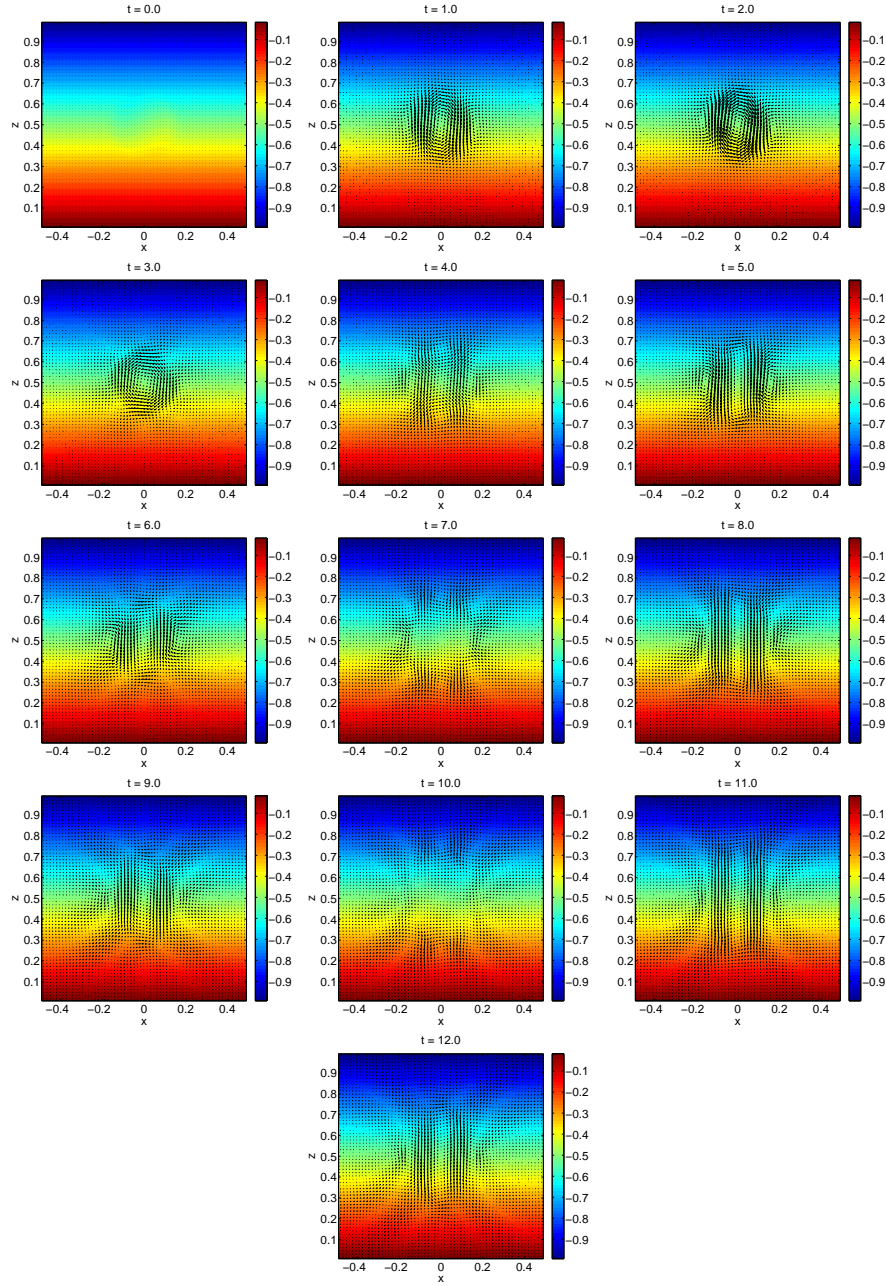


FIGURE 12. Evolution of the buoyancy field with superimposed velocity in the inertially stable case  $\mathcal{R} = 1$ . Emission of inertia-gravity waves due to initial perturbation is clearly seen. The corresponding animation may be viewed at [http://www.geometry.caltech.edu/Movies/BoussinesqAIMS/both4\\_5R1beta1b.avi](http://www.geometry.caltech.edu/Movies/BoussinesqAIMS/both4_5R1beta1b.avi)

vorticity ejected out of the flow in accordance with the convective character of the inertial instability.

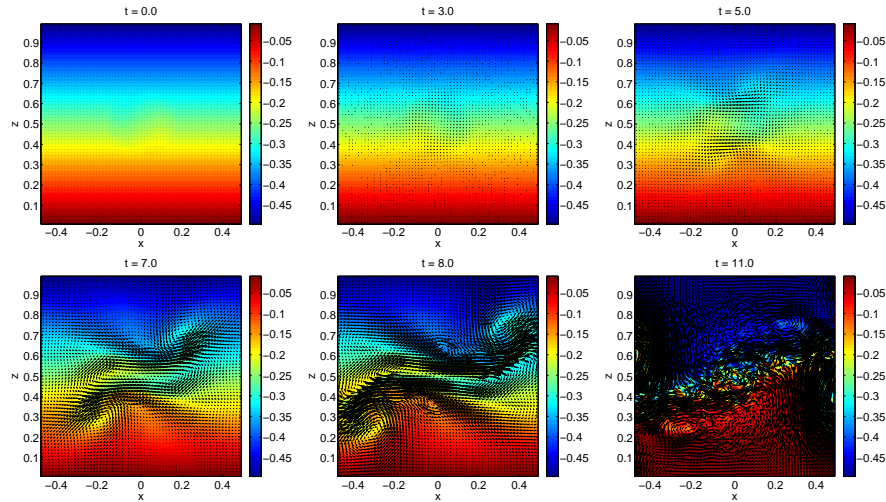


FIGURE 13. Evolution of the buoyancy field (colours) with superimposed velocity in the inertially unstable case  $\mathcal{R} = 2$ . Only the part of the calculational domain around initial perturbation is displayed. The corresponding animation may be viewed at [http://www.geometry.caltech.edu/Movies/BoussinesqAIMS/both4\\_5R2beta05b.avi](http://www.geometry.caltech.edu/Movies/BoussinesqAIMS/both4_5R2beta05b.avi)

This behavior is consistent with the Lagrangian picture of the inertial instability [15] and with the evolution of the periodic perturbations considered in [27]. As seen from the evolution of the geostrophic momentum, this evolution leads to a considerable reorganization of the mean flow, with eventual homogenization of the geostrophic momentum at the location of the perturbation. This is fully consistent with the general scenario of the evolution of inertial instability [20], yet the dissipationless character of the code allows to capture fine details smeared by the dissipation in the existing simulations of the saturation of the inertial instability.

The energy evolution of the system is presented in Fig. 15. As indicated by this figure, the energy is nearly perfectly conserved.

**6.4. Conclusions.** Our numerical tests showed feasibility of efficient numerical implementation of the structure-preserving symplectic integrators for Boussinesq equations of rotating stratified fluids. The slow and the fast components of the flow were correctly reproduced in spite of relatively low resolution; the waves were well simulated, their characteristic properties correctly recovered; and the conservation laws were perfectly verified, with long-term energy conservation. The hard test of inertial instability showed agreement with common knowledge of the instability. As future work, one may want to leverage upwinding techniques to remove numerical artifacts near sharp gradients of buoyancy without interfering with the structure preservation of our update equations.

**Acknowledgments.** The authors thank Jerrold E. Marsden for early inspiration.

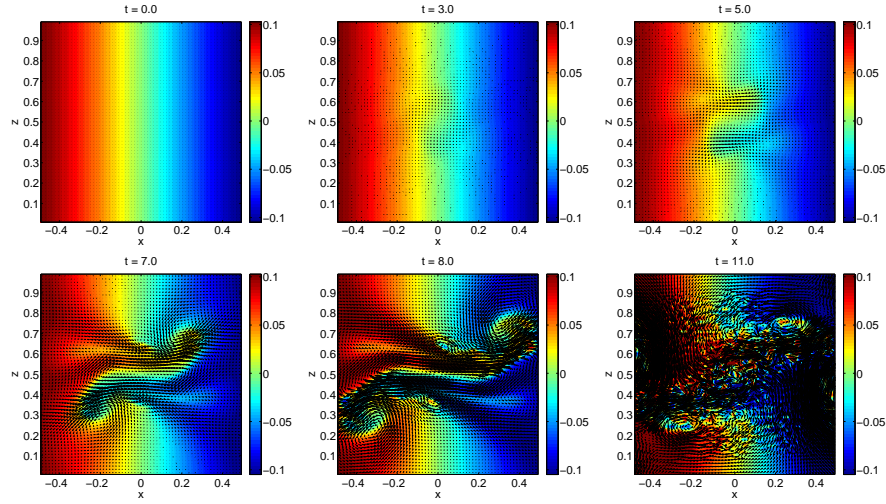


FIGURE 14. Geostrophic momentum (colours) with superimposed velocity in the inertially unstable case  $\mathcal{R} = 2$ . Only the part of the calculational domain around initial perturbation is displayed. The corresponding animation may be viewed at [http://www.geometry.caltech.edu/Movies/BoussinesqAIMS/both4\\_5R2beta05M.avi](http://www.geometry.caltech.edu/Movies/BoussinesqAIMS/both4_5R2beta05M.avi)

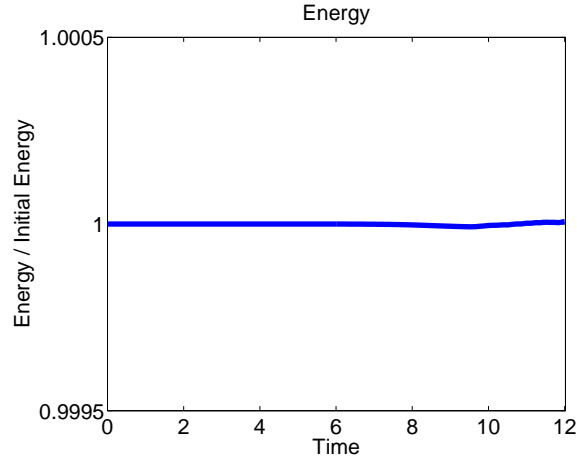


FIGURE 15. Energy behavior in the simulation of the inertially unstable case  $\mathcal{R} = 2$ .

#### REFERENCES

- [1] R.V. Abramov and A. J. Majda, *Statistically relevant conserved quantities for truncated quasigeostrophic flow*, Proc. Natl. Acad. Sci. U.S.A., **100** (2003), 3841–3846.
- [2] V. I. Arnold, *Sur la géométrie différentielle des groupes de Lie de dimension infinie et ses applications à l’hydrodynamique des fluides parfaits*, Ann. Inst. Fourier, Grenoble, **16** (1966), 319–361.
- [3] V. I. Arnold, “Mathematical methods in Classical Mechanics”, Springer, NY, 1974.

- [4] D. N. Arnold, R. S. Falk, and R. Winther, *Finite Element Exterior Calculus, Homological Techniques, and Applications*, Acta Numerica, **15** (2006), 1–155.
- [5] V. I. Arnold and B. A. Khesin, “Topological Methods in Hydrodynamics”, Springer, New York, 1998.
- [6] A. Bossavit, “Computational Electromagnetism”, Academic Press, Boston, 1998.
- [7] N. Bou-Rabee and J. E. Marsden *Hamilton-Pontryagin Integrators on Lie Groups Part I: Introduction and Structure-Preserving Properties*, Foundations of Computational Mathematics, **9**(2) (2008), 197–219.
- [8] M. Desbrun, E. Kanso, and Y. Tong, *Discrete differential forms for computational modeling*, in “Contributions to Nonlinear Functional Analysis” (eds., A. Bobenko and P. Schröder), Springer, 2007.
- [9] E. S. Gawlik, P. Mullen, D. Pavlov, J. E. Marsden, and M. Desbrun *Geometric, variational discretization of continuum theories*, Physica D, **240**(21), (2011), 1724–1760.
- [10] I. Gjaja and D. D. Holm, *Self-consistent Hamiltonian dynamics of wave mean-flow interaction for a rotating stratified incompressible fluid* Physica D, **98**(2) (1996), 343–378.
- [11] E. Hairer, C. Lubich, and G. Wanner “Geometric numerical integration, Structure-preserving algorithms for ordinary differential equations”, Springer-Verlag, Berlin, 2006.
- [12] F. H. Harlow and J. E. Welch *Numerical calculation of time-dependent viscous incompressible flow of fluid with free surface*, Physics of Fluids, **8**(12), (1965), 2182–2189.
- [13] D. D. Holm, J. E. Marsden and T. S. Ratiu, *The Euler-Poincaré equations and semidirect products with applications to continuum theories* Adv. in Math., **137** (1998), 1–81.
- [14] D. D. Holm and V. Zeitlin, *Hamilton’s principle for quasi-geostrophic dynamics*, Phys. Fluids, **10** (1998), 800–806.
- [15] J. R. Holton, “An introduction to Dynamic Meteorology” third edn., Academic Press, 1992.
- [16] B. J. Hoskins, M. E. McIntyre, and A. W. Robertson, *On the use and significance of isentropic potential-vorticity maps* Q. J. R. Met. Soc., **111** (1985), 877–946.
- [17] H. Lamb, “Hydrodynamics”, Ch. 309, 310, Dover, 1932.
- [18] J. Lighthill, “Waves in Fluids”, Ch. 4, CUP, 1978.
- [19] B. Kadar, I. Szunyogh, and Q. J. Devenyi *On the origin of model errors*, J. Hung. Meteor. Soc., **101** (1998), 71–107.
- [20] R. C. Kloosterziel, P. Orlandi, and G. F. Carnevale *Saturation of inertial instability in rotating planar shear flows*, J. Fluid Mech., **583** (2007), 413–422.
- [21] J. E. Marsden and T. S. Ratiu, “Introduction to Mechanics and Symmetry” Springer (1999).
- [22] J. E. Marsden and M. West *Discrete mechanics and variational integrators*, Acta Numer., **10** (2001), 357–514.
- [23] J. Marshall and F. Molteni *Toward a dynamical understanding of planetary-scale flow regimes*, J. Atmos. Sci. **50** (1993), 1792–1818.
- [24] S. Medvedev and V. Zeitlin [2010], *Parallels between stratification and rotation in hydrodynamics, and between both of them and external magnetic field in magnetohydrodynamics, with applications to nonlinear waves*, IUTAM Bookseries, **28** (2010), 27–37.
- [25] D. Pavlov, P. Mullen, Y. Tong, E. Kanso, J. E. Marsden, and M. Desbrun *Structure-preserving discretization of incompressible fluids*, Physica D, **240**(6) (2010), 443–458.
- [26] J. Pedlosky, *Geophysical Fluid Dynamics*, Springer, NY, 1979.
- [27] R. Plougonven and V. Zeitlin *Nonlinear development of inertial instability in a barotropic shear*, Physics of fluids, **21** (2009), 106601.
- [28] R. Salmon, “Lectures on Geophysical Fluid Dynamics”, OUP, NY.
- [29] V. Zeitlin, G. M. Reznik, and M. BenJelloul, *Nonlinear theory of geostrophic adjustment. Part 2. Two-layer and continuously stratified primitive equations*, J. Fluid Mech. (2003), **491**, 207–228.

E-mail address: [mathieu@caltech.edu](mailto:mathieu@caltech.edu)

E-mail address: [egawlik@stanford.edu](mailto:egawlik@stanford.edu)

E-mail address: [francois.gay-balmaz@lmd.ens.fr](mailto:francois.gay-balmaz@lmd.ens.fr)

E-mail address: [zeitlin@lmd.ens.fr](mailto:zeitlin@lmd.ens.fr)